DEVELOPMENT OF INKS FOR 3D PRINTING OF BLOCK COPOLYMER SELF-ASSEMBLY DIRECTED HIERARCHICALLY STRUCTURED OXIDES

A Thesis

Presented to the Faculty of the Graduate School

of Cornell University

In Partial Fulfillment of the Requirements for the Degree of

Master of Science

by

Sejal Sanjeev Sheth

August 2023

ABSTRACT

The 3D printing technique of Direct Ink Writing (DIW) allows the fabrication of functional materials of various form factors and geometries. Combining this technique with inks made from block copolymer (BCP) self-assembly directed inorganic precursors provides access to hierarchically ordered hybrids. Through subsequent thermal processing, such hybrids can be converted into functional materials for applications ranging from catalyst supports to quantum information science. Here, the development of alcoholic inks for DIW is discussed that consist of Pluronics family block copolymers and sol-gel precursors for various transition metal oxides, i.e., niobia and titania. Thin film experiments guide the choice of the ink composition and rheological studies guide the choice of the ink composition and mode of DIW printing into woodpile lattice structures. Resulting as-made hybrids and final oxides are characterized by a combination of small-angle and wide-angle x-ray scattering, scanning electron microscopy, and nitrogen sorption. Finally, in the case of niobia based woodpile structures, further conversion into niobium nitride is demonstrated via thermal processing in ammonia. Such nitrides, once optimized for the right crystal size, demonstrate superconductivity. This opens pathways to the direct printing of quantum materials with arbitrary form factors and well-defined mesostructures from BCP self-assembly leading to quantum metamaterials behavior.

BIOGRAPHICAL SKETCH

Sejal Sheth's early years were spent in Alibaug, Maharashtra, a coastal town in western India renowned for its pristine beaches. Due to her father's job transfers, she experienced living in three different states and changed schools on five occasions. In her family, she is accompanied by her younger sister, as well as her mother, a doctor, and her father, a chemical engineer. Inspired by her father's profession, Sejal made the decision to pursue a career in Chemical Technology.

Sejal's educational journey led her to the prestigious Institute of Chemical Technology (ICT) in Mumbai, India, where she enrolled in their chemical engineering program. During her freshman year at ICT, she had a remarkable opportunity to present a poster at Vortex, India's largest ChemFest, which was organized by the institute. Her presentation centered around the field of Nanotechnology, specifically focusing on 'Molecular Machines,' an area that had recently been awarded the Nobel Prize. This experience ignited her fascination with nanomaterials and nanotechnology, prompting her to delve deeper into the subject through extensive reading and enrollment in relevant courses. It was during this time that Sejal decided to pursue a master's degree in Materials Science and Technology, with a specific focus on nanotechnology. In 2021, she joined the MSE program at Cornell University to pursue her dream.

Dedicated to a better and sustainable future.

ACKNOWLEDGMENTS

I would like to express my sincere gratitude to my incredibly knowledgeable advisor, Prof. Ulrich Wiesner. His support, guidance, and wisdom throughout my master's program have been invaluable. I am also deeply grateful to Prof. Lara Estroff, who has generously shared her knowledge and expertise with me as a committee member.

I would like to extend a heartfelt thank you to my mentor, Fei Yu, for his patient guidance and assistance throughout my research, including helping me through challenging times and providing valuable academic and non-academic feedback. I would also like to acknowledge the other members of my group, including Lilly Tsaur, William Tait, William Moore, and the entire lab group, for their assistance with sample characterization, patient responses to my inquiries, and unwavering support.

Most importantly, I am immensely grateful to my parents, Sanjeev and Shreya, my sister Siddhi, and my grandparents for their unconditional love and unwavering encouragement. Their support has made it possible for me to pursue my studies at my dream university. I would also like to express my gratitude to my boyfriend, Sachin, for guiding me in MATLAB and being a constant source of support through both difficult and joyful times. Finally, I would like to thank all my friends and seniors, both at Cornell and back in India, for always being there for me.

TABLE OF CONTENTS

LIST OF FIGURES

LIST OF TABLES

LIST OF ABBREVIATIONS

DIW	Direct Ink Writing
TTIP	Titanium tetraisopropoxide
SEM	Scanning Electron Microscopy
SAXS	Small Angle X-Ray Spectroscopy
WAXS	Wide Angle X-Ray Spectroscopy
XRD	X-Ray Diffraction
MOs	Metal Oxides
PEO	Polyethylene Oxide
PPO	Polypropylene Oxide
BCPs	Block Copolymers
CHESS	Cornell High Energy Synchrotron Source
LVE	Linear Viscoelastic Region
AM	Additive Manufacturing

Chapter 1: Introduction and Background

1.1 Introduction

Materials exhibit distinct behaviors at the nano- and mesoscale compared to their bulk counterparts.[1] Among the various routes to nanomaterials, the self-assembly of block copolymers (BCPs) presents a facile and tunable pathway based on solution processing. In addition, BCPs can structure-direct the arrangement of the desired materials, such as functional inorganics that lack access to well-defined mesostructures. The organic BCPs can be removed through processes such as calcination, resulting in the formation of mesoporous inorganic structures. The presence of these mesoporous structures arises due to the nanoscale size of the polymers. By carefully selecting the chemistry, architecture, and dimension of the BCPs, it is possible to tune the pore size and the periodic spacing (d-spacing). Although there are alternative top-down deposition techniques that can produce nanometer and submicrometer structures, their requirement for specialized equipment and typically high vacuum makes the process expensive and less accessible. In contrast, BCP self-assembly combined with sol-gel chemistry[2] is versatile, scalable, and cost-effective.

Moreover, nanomaterial fabrication is known to be plagued by low throughput and limited form factors. To leverage the intriguing properties displayed by the nano- and mesostructures with scalability to the bulk or other form factors, the advent of 3D printing now makes it feasible to scale up and extend to diverse form factors and intricate geometries while retaining the mesoscale characteristics, all through solution-based processes. This presents new opportunities to explore a wide range of materials with tailored structures across many length scales for applications including energy conversion and storage, catalysis, and even information technology.

The present study focuses on the 3D printing of BCP-directed transition metal oxides, with particular emphasis on niobia. The investigations were subsequently extended to titania, another transition metal oxide, to demonstrate the versatility of this approach. As a functional example, niobium oxides, when converted to niobium nitride by the ammonolysis method[3] are superconductive, with potential applications in various fields such as superconducting electronics or quantum computing[4]

1.2 Background

Recent research advancements have addressed challenges including the synthesis of ordered mesoporous materials. Novel approaches using block copolymers (BCPs)[5] have allowed for greater control over mesostructure formation, enabling the precise tuning of pore size and interconnectivity. Moreover, advancements in sol-gel chemistry[2] have provided a simpler, more versatile, and cost-effective route for mesoporous material synthesis compared to traditional deposition techniques.

Furthermore, the emergence of 3D printing[6] technologies has revolutionized materials fabrication, offering high flexibility in designing complex geometries and diverse form factors. This advancement allows for the creation of customized mesoporous structures tailored to specific applications, such as fuel cells, separation membranes, catalysis, and superconductors.[7]

Building upon this background, the research described in this thesis focuses on exploring the application of 3D printing for the fabrication of BCP directed ordered mesoporous transition metal oxides to generate functional materials of intricate geometries.

1.2.1 3D Printing

Compared to conventional methods that are often subtractive in nature such as carving or lithography, 3D printing, also known as additive manufacturing, of soft polymer-based materials offers rapid prototyping and customization for various applications. In the simplest setup, the designed objects are "printed" in a layer-by-layer fashion according to the data from 3D computer models. There are various 3D printing techniques available today, some of which are illustrated in Fig 1.1.

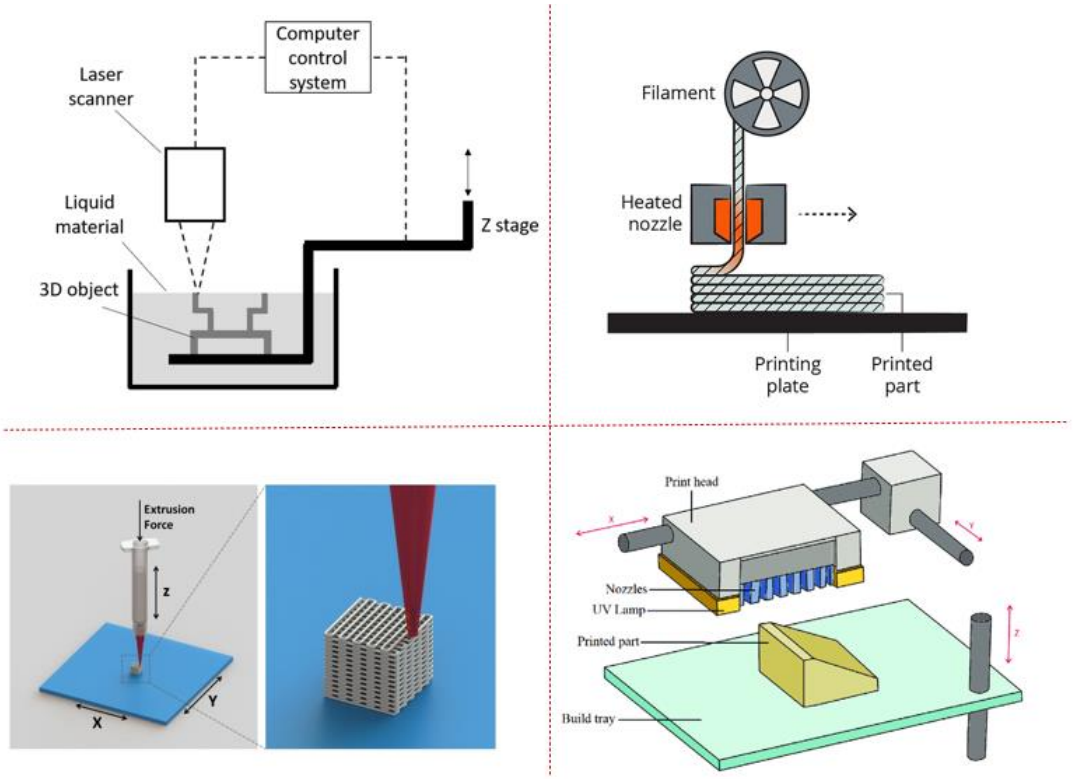

Fig 1.1: Schematic illustration of different 3D printing techniques for polymers including (a) stereolithography[25], (b) fused deposition modeling[26], (c) direct ink writing[27], and (d) polyjet printing[28]

While significant research has been conducted on 3D printing of polymeric materials and simple inorganic materials such as ceramics, silica[6] and mesoporous bioactive glasses[8], there is currently a gap in the literature regarding the printing of transition metal oxides with well-defined mesostructures. This particular research area holds

substantial interest due to the unique functionalities these materials offer, both in their oxide form and when converted into other materials such as nitrides. To the best of our knowledge, no published studies have investigated the 3D printing of these mesoporous transition metal oxide materials through a self-assembled pathway. Addressing this gap would unleash new functionalities as a result of previously unknown properties due to limitations in manufacturing and expand the potential applications of mesoporous materials in various fields.

Direct ink writing (DIW)[9] is an extrusion-based additive manufacturing technique used to pattern functional materials with intricate geometries and complex form factors. It is a versatile method applicable to a wide range of material compositions including polymers, ceramics, glass, cement, graphene, and metals, and does not require intricate instrumental designs. The viscoelastic ink, typically a solution or slurry, is extruded through a nozzle and deposited in a layer-by-layer pattern, which is deposited on a platform controlled to move in an x-y direction resulting in 3D scaffolds. Inks for DIW include, but are not limited to, colloidal solutions, functional composites, fugitive organic inks, and polyelectrolyte inks.[10] The advantages of using this technique are the flexibility in materials choice, low cost, scalability, iterative design, integration of functional elements, and rapid prototyping. The key requirement is that the inks need to exhibit shear-thinning-type viscoelastic properties[11] so that the ink restores the mechanical strength once extruded out of the nozzle. There are two approaches in DIW, namely, droplet and filament based. This work explores the filament-based approach where ink is continuously extruded through a fine cylindrical nozzle forming filaments that are laid down in a layer-by-layer fashion.[12]

1.2.2 Block Copolymer Self-Assembly

Block copolymers (BCPs) and their self-assembly serve as highly versatile structure directing agents for the creation of mesostructured and mesoporous materials, offering the ability to precisely tune morphology, pore size, and wall thickness [5]. Supramolecular structures, including those of surfactants and BCPs, provide an organic approach to achieving mesoscale order in materials. Among these, diblock and triblock copolymers are commonly employed as BCP-based structure directing agents. The resulting morphologies obtained from BCP self-assembly directed inorganic materials formation via the sol-gel process depend on factors such as the hydrophilic/hydrophobic nature of the polymer, the shape of the polymer, the degree of polymerization, and the polymer-to-sol nanoparticles ratio. By carefully controlling these parameters, a wide range of morphologies can be achieved, allowing for tailored structures in mesostructured and mesoporous materials.

Pluronics, also known as Poloxamers or Synperonics, are commercially available amphiphilic triblock copolymers, $(PEO)_n$–$(PPO)_m$–$(PEO)_n$, consisting of symmetrical more hydrophilic poly(ethylene oxide) end blocks synthesized from ‘n’ EO units at both ends and a more hydrophobic poly(propylene oxide) middle block derived from ‘m’ PO units. In aqueous solutions Pluronics family BCPs form micelles, in which the PEO blocks occupy the corona whereas the PPO block resides in the core [13], [14] to conventional nonionic surfactants. Various mesostructures can be self-assembled by Pluronics, such as hexagonal, cubic, and lamellar liquid crystalline phases at high concentrations.

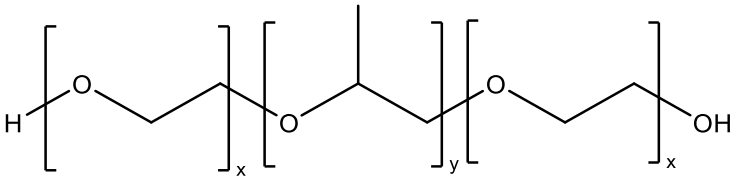

Fig 1.2: Structure of a Pluronic block copolymer

Pluronics, being small-sized polymers, can be seamlessly blended with other components in both aqueous and alcoholic solutions. This characteristic makes them ideal for formulating inks specifically designed for DIW printers, which typically cannot accommodate inks based on organic solvents.

The co-assembly of BCPs, a supramolecular structure directing agent, and a transition metal precursor by sol-gel condensation gives rise to mesoporous metal oxides when calcined. Using Pluronics as BCPs gives mesostructures with a wall thickness typically between 50 Å and 100 Å.[15] Direct ink writing of these inks provides and additional layer of macroscale control to final printed structures. The mesostructure control arising from BCP self-assembly and the macrostructure control arising from DIW together give rise to hierarchically porous structures.[16] This hierarchical porosity of transition metal oxides renders them functional metamaterials of high interest with properties that deviate from their bulk behavior.

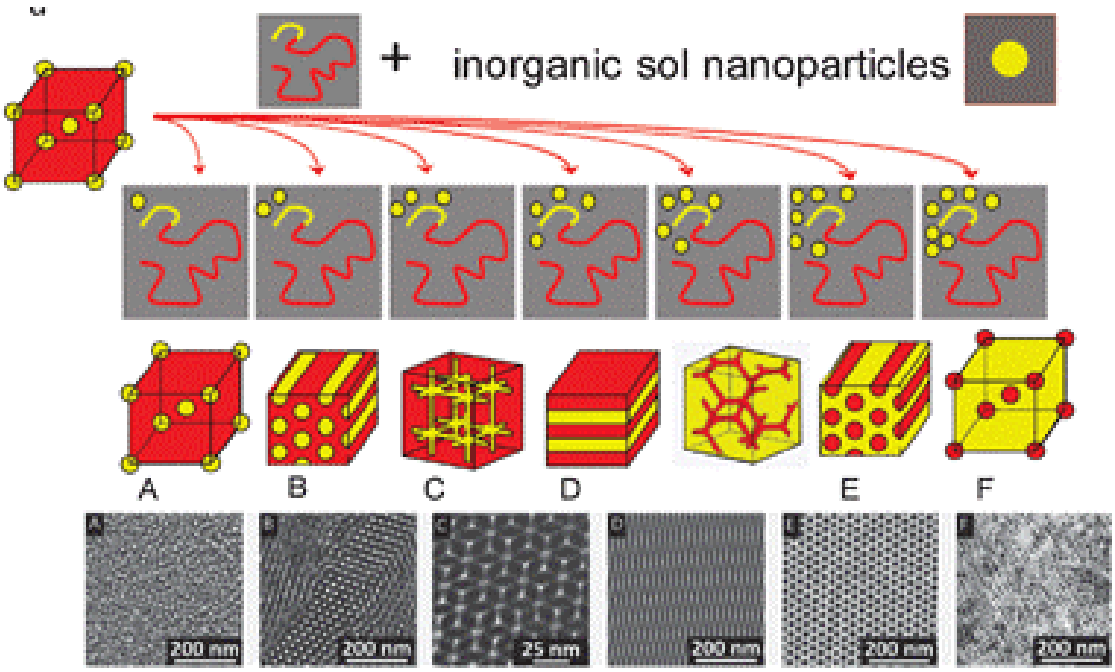

Fig 1.3: Organically modified metal oxide hybrid morphologies as a result of increasing volume fractions of inorganic material precursors added to a diblock copolymer as a structure-directing agent.[29]

The motivation behind using Pluronics is that they are compatible with DIW equipment, whereas conventional BCPs, typically of larger molar mass than Pluronics polymers, require organic solvent systems that may dissolve/degrade specific printer parts. Pluronics with varying molar masses and block ratios are commercially available as displayed in Figure 1.4. Specific Pluronics BCPs F127 and P123, of high and medium molar mass, were explored in this work to prepare inks for DIW.

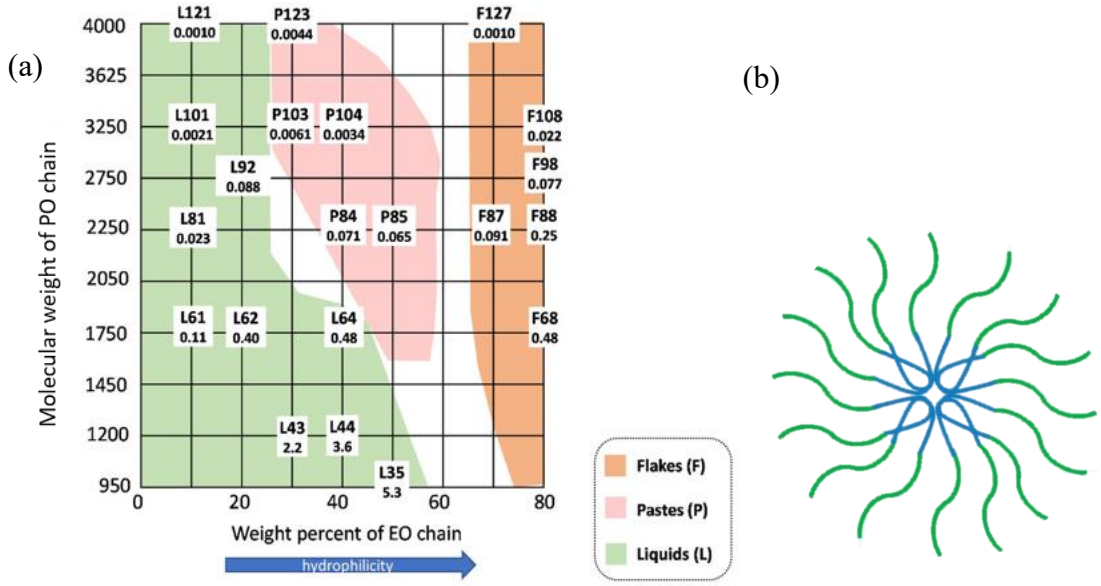

Fig 1.4: (a) Hydrophilic lipophilic balance (HLB) grid for Pluronics series polymers[30]. (b) Schematic of a Pluronics BCP micelle in water/aqueous solutions.

1.2.3 Pluronic Ink System to Structure-direct transition metal oxides

Studies in the past established mesoporous metal oxide (MO) structures of different morphologies including hexagonal and cubic mesophases directed by a range of different Pluronics.[17] The sol-gel solution used in this study comprises several key components [16]. The Pluronics family BCP serves as an agent for directing the organization of sol-gel derived transition metal oxide nanoparticles. Ethanol, an

amphoteric solvent, is utilized to ensure the solubility of all precursors involved in the sol-gel process. A transition metal precursor, typically a metal alkoxide, undergoes hydrolysis/alcoholysis through stirring to convert it into metal oxide sol nanoparticles. In the case of F127-niobia inks, niobium (V) ethoxide was employed as the transition metal precursor. Acetic acid, AcOH, a capping agent, is incorporated into the solution to modify the condensation kinetics of the metal alkoxides. Lastly, HCl, a strong aqueous acid, is introduced to catalyze the partial hydrolysis of the inorganic precursor and enhance its affinity towards the hydrophilic block of the BCP.

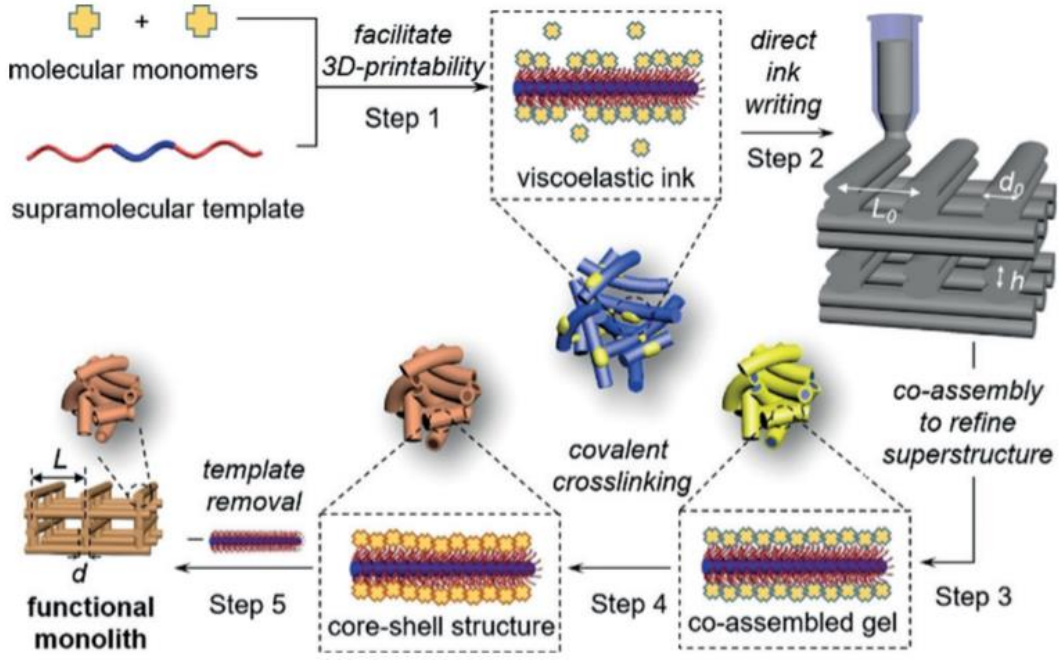

Fig 1.5: Co-assembly enhanced direct ink writing [16]

Previous work has reported on inks composed of pluronic-type BCP directed mesoporous silica[16] whose sol-gel transition kinetics is orders of magnitude slower than that of transition metal oxides. 3D printing is a continuous process taking place over a specific period of time. Therefore, the challenge is to ensure the window for processing the transition metal oxide sol-containing ink matches the timescale of printing. There are studies that in the past have successfully explored and prepared

different mesoporous metal oxides by tuning the mixture compositions.[18] The additive AcOH modifies and slows down the condensation kinetics of metal alkoxides giving better control over the structural order of the resulting mesoporous materials.

To print these inks, they should show a shear thinning behavior, while their modulus should be in a particular regime that enables successful printing of the inks without losing structural control of the printed parts as discussed in the supporting information of a study by Li *et al*.[19] In order to check for those properties one can use dynamic mechanical analysis of the inks. From such measurements, the storage modulus (G') represents the elastic response while the loss modulus (G'') represents the viscous response of the viscoelastic properties by such inks. As will be shown in the next sections, those properties need to be optimized for the present BCP/transition metal oxide-based inks to provide access to DIW printed parts for good structure control.

Chapter 2: Experimental Methods and Characterization

2.1 Experimental Procedure

2.1.1 Optimizing the Ink Composition

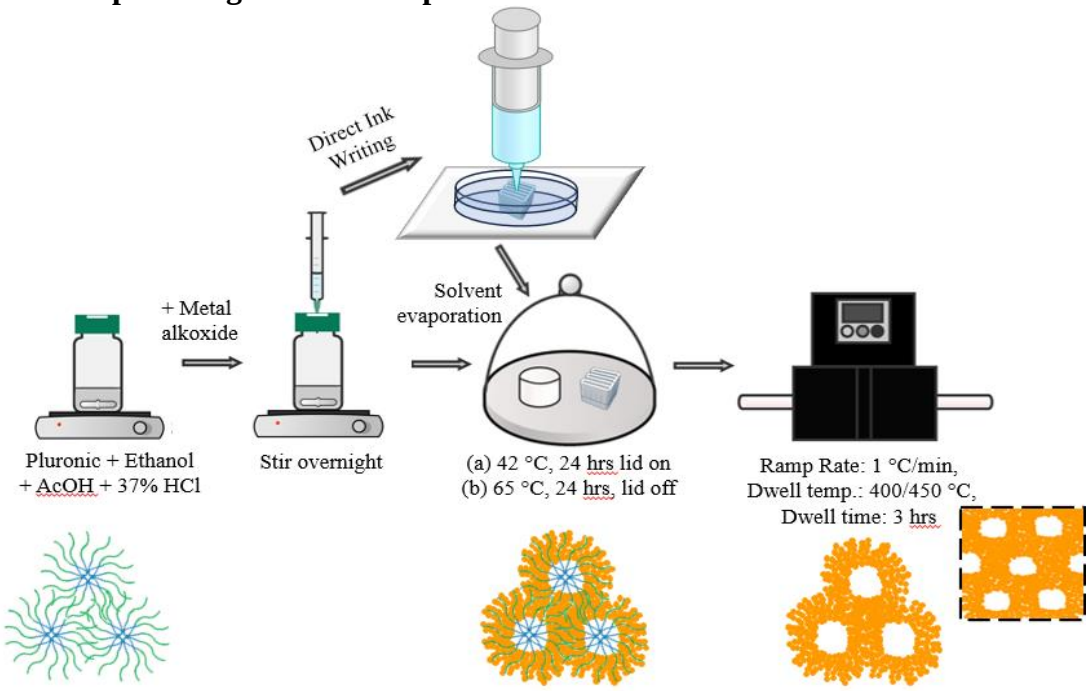

Fig 2.1: Pluronics BCP self-assembly derived sol-gel metal oxide thin films and 3D printed woodpile structures. Dwell temperature is dependent on the transition metal oxide.

Referring to the previous literature on F127-directed niobia mesoporous structures, [15], [20] studies started by preparing dilute inks for evaporation-induced self-assembly to figure out the approximate range of compositions before undertaking actual 3D printing experiments, which consumes a lot of material. Precursor and acid ratios with respect to Pluronics BCS were varied in the film formation step. Scanning electron microscopy, SEM, images on calcined samples subsequently guided the choices for solution compositions towards the direction of the desired morphology. A step-by-step process was followed as shown in Figure 2.1 to prepare mesoporous thin films. The illustration shows cylindrical micelles formed in aqueous/alcoholic solutions with PEO corona block and PPO core blocks of the BCPs (*vide supra*).

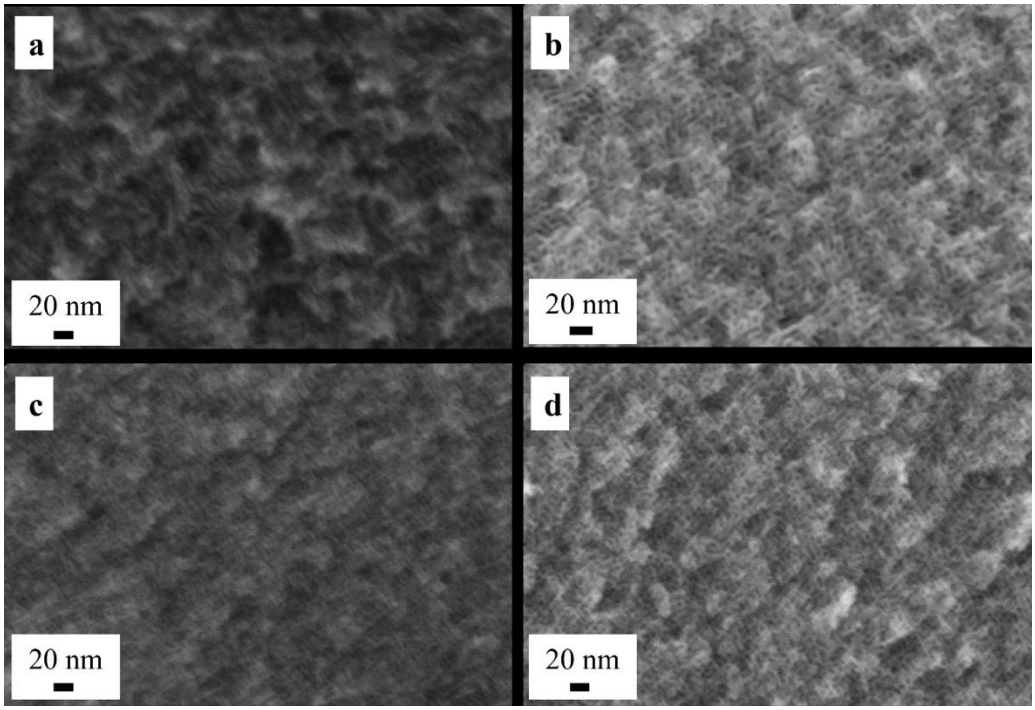

Fig. 2.2: Representative examples of SEM images of mesostructured niobium oxide thin films. Inks were made with varying compositions, changing the amounts of acids and metal precursor to find the right recipe to achieve an ordered hexagonal morphology. Maintaining a constant amount of Pluronic and ethanol, the quantities of niobium alkoxide, HCl, and AcOH were varied in ascending order from 'a' to 'd', proportionally.

Table 2.2: Composition of ink for Pluronic-directed MO thin films.

Pluronic-Metal Ink Type	**Pluronic (g)**	**Ethanol (ml)**	**Glacial Acetic Acid (µL)**	**37 wt% aq. HCl (µL)**	**Metal Alkoxide precursor (ml)**
F127-Niobia	**F127** 0.4	8	285.5	185.5	**$Nb(OEt)_5$** 0.625
P123-Niobia	**P123** 0.4	8	308.3	201.7	**$Nb(OEt)_5$** 0.675
F127-Titania	**F127** 0.4	8	285.5	186.8	**TTIP** 0.76

In a particular successful example, in a vial, 400 mg of Pluronic F127 was dissolved in around 8 ml ethanol. To this mixture, 285.5 µL of glacial acetic acid and 185.5 µL of 37 wt% HCl were added and vigorously stirred until the solution became transparent. 0.625 ml niobium (V) ethoxide was injected unto the vial and the resulting solution was stirred vigorously overnight for ~ 12 hrs to allow for the sol-gel process to occur. Under these conditions, the niobium ethoxide precursor hydrolyzes/condenses to form nanosized metal-oxo-acetate sol nanoparticles in the AcHE solution as reported previously.[15] The next day, these solutions were poured into Teflon cups covered with a glass dome and evaporated at 42 °C for ~24 hrs followed by further aging at 65 °C in an oven for another ~24 hrs. The as-synthesized mesostructured thin films were calcined in a furnace in air at 450 °C, with a ramp rate of 1°C/min and dwell time of 3hrs to decompose the Pluronics BCP and other organic matter resulting in mesoporous and amorphous niobium oxide structures.

Once a range of compositions resulting in the desired hexagonal morphology control were determined, rheology experiments of these inks were performed in order for the viscoelastic properties of these solutions to be in the printable regime as reported by Li *et al.* [16].

2.1.2 Direct Ink Writing

The aim of this work was to print a so called woodpile lattice as schematically shown in Fig. 2.1. The woodpile geometry was selected because it gives rise to the desired macroscale porosity which when combined with BCP-directed mesoporosity would give rise to hierarchically porous structures. The requirement for good 3D printed structures by DIW is that these metal oxide sol precursor-BCP based solutions should readily deform upon the forces of extrusion while forming a stable structure once the ink has been deposited during DIW. During and after 3D printing, the solvent

evaporation-induced self-assembly and further calcination for template removal, respectively, result in the desired periodically ordered mesostructure that constitutes the printed woodpile lattice structure of the final metal oxide.

For each ink system, various parameters had to be optimized, such as print head speed, ink extrusion rate, and the utilization of a solvent bath. To successfully print the ink compositions listed in Table 2.1, which exhibited desirable mesostructures, it was necessary to further concentrate the inks by reducing the ethanol content. To determine the appropriate printing parameters, a series of rheology experiments were designed, providing qualitative insights that aided in the decision-making process.

2.2 Characterization Techniques

2.2.1 Small-Angle X-Ray Scattering (SAXS)

Ex-situ transmission SAXS at the Cornell High Energy Synchrotron Source (CHESS) and at the National Synchrotron Light Source II (NSLS-II) was used to characterize the morphology of the polymer-inorganic hybrids and the resultant metal oxide structures after calcination. The energy of the X-ray at CHESS was 11.24 keV and the energy at NSLS-II was 16.1 keV. The relative peak positions of Bragg reflections (q/q^*) reveal the type of mesostructure with a specific symmetry while shifts in peak positions suggest changes in d spacing between samples at different stages of processing.

2.2.2 Wide-Angle X-Ray Scattering (WAXS)

To probe amorphous or crystalline metal oxide structures at the atomic scale, WAXS data for the niobia and titania woodpiles were collected at CHESS and NSLS-II. In addition, a lab-based Bruker D8-ECO powder x-ray diffractometer using Cu Kα radiation was also employed to analyze titania thin films.

2.2.3 Nitrogen Sorption

Nitrogen sorption measurements were performed using a Micromeritics ASAP 2020 surface area and porosity analyzer at 77K. The samples were loaded in clean oven-dried glass tubes and degassed under vacuum at 120 °C for ~12hrs before performing measurements. Nitrogen sorption was used to find the specific surface area and pore size distribution of the printed mesoporous materials. The shape and character of the isotherms provide further information on the accessibility and connectivity of pores.

2.2.4 Scanning Electron Microscopy (SEM)

A Zeiss Gemini 500 SEM was used to characterize all samples. Samples were mounted such that their freshly cracked cross-section was pointing upwards. There was no need to sputter coat the samples before acquiring images. An accelerating voltage of 2 kV was used. SEM images provided a visual check on which ink composition was suitable to give the best morphology and also served to corroborate the d spacings and pore sizes obtained from SAXS and nitrogen sorption data, respectively.

2.2.5 Rheology

Rheology experiments were performed using a TA instruments DH3 rheometer. Cone-plate geometry of diameter 40mm and truncation 63 μm was used. This geometry is meant to provide a constant shear rate, regardless of the distance from the center of the plate. While performing the rheology measurements, the bottom plate is stationary and the top plate moves and is responsible for providing shear stress on the ink or any test sample. During the rheology measurements, the gap between the two plates is maintained by default at 63 μm, referred to as the truncation gap (i.e., the truncation height of the top cone plate) in this thesis. Approx. 1 ml of the ink sample was spread on the surface of the bottom plate using a dropper. This plate was then brought into

contact with the top plate so that both plate surfaces were evenly covered with the sample. This first step was followed for all the rheology measurements performed on inks studied for this thesis.

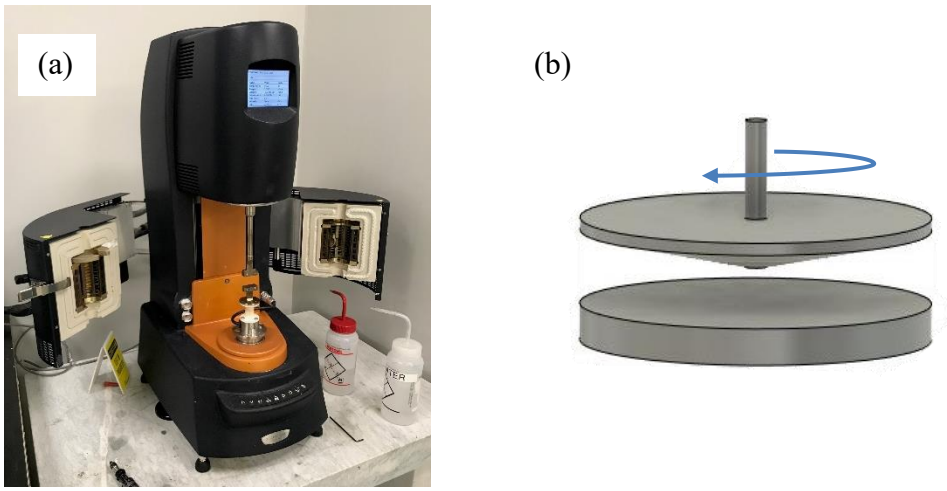

Fig 2.3: (a) An image of a TA instruments DH3 rheometer, and (b) a schematic of the cone and plate rheometer geometry

To check whether the viscolastic properties of the inks studied were suitable for DIW as described in the literature, the following rheology measurements were performed:

(a) Oscillatory Tests

i. Strain/Amplitude Sweep

ii. Frequency Sweep

(b) Flow Ramp

(a) Oscillation Tests:

Oscillatory measurements provide information on the viscoelastic properties in the linear regime, also known as the linear viscoelastic region (LVR). *Amplitude sweeps* show the extent to which the material exhibits linear viscoelastic behavior and determine the highest critical strain beyond which the material shows non-linear behavior (i.e., shear thinning). *Frequency sweeps* test the viscoelastic behavior of a material at

different shear rates under shear at a given shear amplitude, γ_A. Polymer materials exhibit various relaxation processes that involve segmental or chain relaxations. A frequency sweep helps to identify these relaxation processes.

(b) Flow Ramps:

Flow ramps are useful to study the non-linear regime and involve applying a controlled and gradually increasing flow rate or shear rate (Figure 2.4). The resulting response is measured in terms of viscosity or shear stress. In the non-linear regime, the relationship between stress and strain is studied to explain the shear thinning phenomenon.

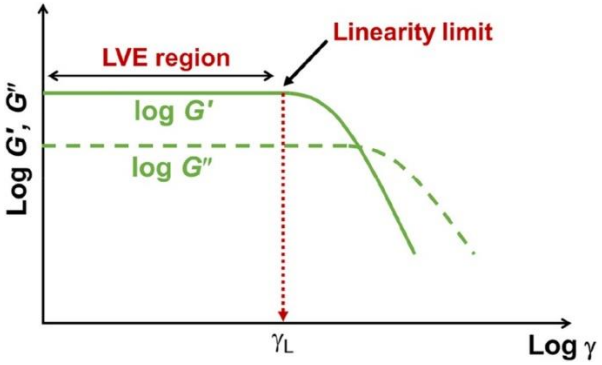

Fig 2.4: The storage and loss modulus displaying a constant value in the linear viscoelastic region (LVR) in a strain amplitude sweep test[21]

Figure 2.5 shows the typical viscoelastic behavior of a polymer as a function of the timescale over which the shear is applied (in terms of frequency). While the Rouse model applies to non-entangled polymer melts, the Zimm model would be applicable to our polymer solution-based inks. It includes the long-range hydrodynamic drag. The relaxation kinetics are faster in polymer solutions, with a smaller rubbery plateau region as it quickly reaches the terminal region. The length of this plateau relates to the molecular weight of the polymer and its concentration in the solution as both these parameters correspond with the number of entanglements and the resulting relaxation time.[22]

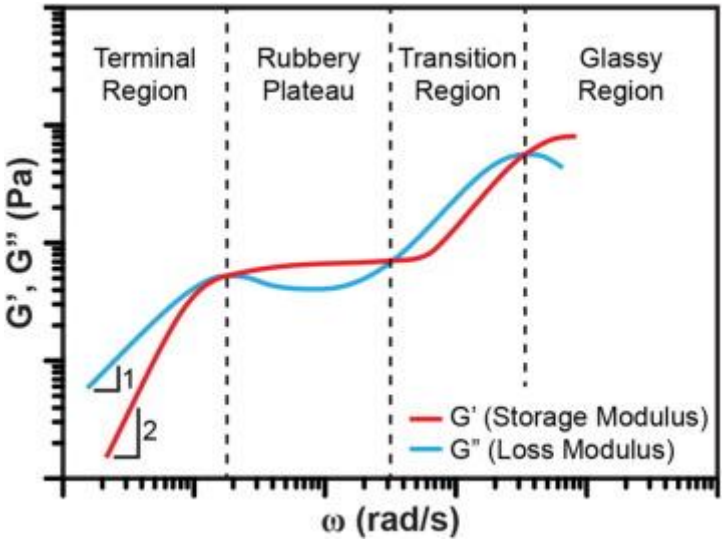

Fig 2.5: The viscoelastic behavior of a polymer solution as a function of the timescale over which shear is applied[22]

For low molecular weight and low concentration polymeric solutions, like in the samples prepared in this work, the important dynamics are expected to occur at shorter timescales, or in other words, the measurements need to be done at higher frequencies.

Chapter 3: Inks for Pluronic-directed Metal Oxides

3.1 F127-directed niobia inks and 3 printed structures

Pluronic F127 is a flaky polymer consisting of PEO blocks on both ends, each consisting of 100 EO units, and a PPO block in the middle consisting of 65 PO units. The molar mass of the polymer is 12,500 g/mol. It forms spherical and cylindrical micelles in aqueous and alcoholic solutions, with PPO blocks in the core and PEO blocks in the corona.

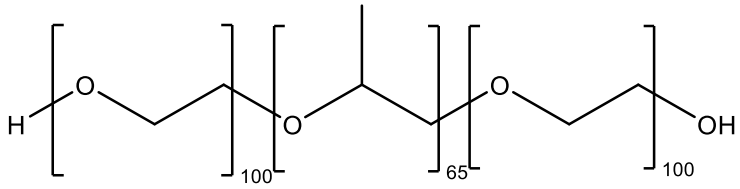

Fig 3.1: Schematic of a Pluronic F127 block copolymer.

3.1.1 Result and Discussion

A. Rheology

Initial rheology experiments were performed directly on the prepared ink. This ink had a very low storage modulus (Figure 3.2a). In fact, it is worthwhile to observe that that under these conditions the storage modulus (G') is lower than the loss modulus (G"). This indicated a more liquid-like behavior of the ink. Although this enhances the extrusion process by increasing the flowability of the ink, it reduces the structural integrity of the printed material. The printed structure's shape fidelity is expected to be compromised as a result of susceptibility to deformation and failure under its own weight. This resulted in low-quality woodpiles or even puddles of inks formed following printing as shown in Figure 3.2c. While the liquid-like behavior of this ink was appropriate for extrusion through the nozzle, once extruded the ink failed as it did not retain the printed structure. It needed further treatment or external support to retain the printed structure.

For subsequent experiments rheology plates covered in ink were left open in air for a specific amount of time, – 5min and 10mins, respectively – and then characterized via rheology. Although there was a significant increase in the moduli (Figure 3.2a,b), the change was not large enough for the viscoelastic ink properties to fall into the required window for printing, as indicated by a pink ribbon in Figure 3.2b below. Although viscoelastic properties improved, with the storage modulus now being higher than the loss modulus when left in air for longer time durations, the printed structures were not strong enough to be self-supporting (Figure 3.2c). It is apparent that leaving it in the air for higher amounts of time (which could have been achieved through slower printing speed in the 3D printing setup) does not yield a printable system.

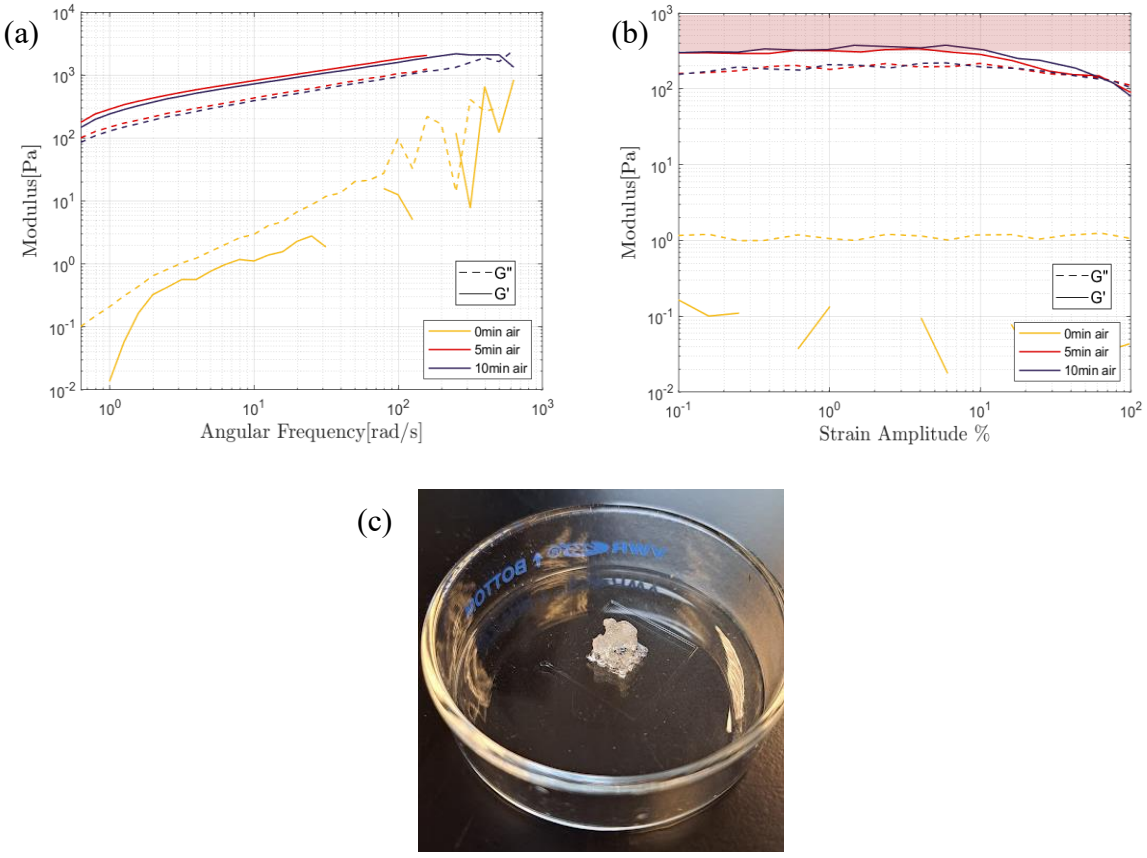

Fig 3.2: Modulus of F123-niobia inks exposed to air for different time spans as measured via (a) frequency sweep and (b) amplitude sweep rheological tests. (c) Image of a printed woodpile leading to crumbling of the structure as a result of the weak viscoelastic properties.

A general workaround to obtain desired viscoelastic properties would be to change the polymer concentration in the solution or to add rheological modifiers. However, the utilization of BCPs as the structure-directing agent places certain restrictions on the ink composition since the BCP chemistry has been fixed and the ratio between BCP and additives cannot be arbitrarily altered when targeting specific self-assembled mesostructures. As an alternative, changing the printing environment may lead to enhanced printed structures as the modulus increase due to the concentration increase solely via evaporation in air is too slow. To improve the viscoelastic properties of the ink and lead to stable structures, as a next step it was therefore thought to print the structures into a non-solvent bath where the liquid-liquid exchange would result in partial precipitation of the Pluronics as well as the sol, a process that could be fast enough to raise the moduli to the level of the printing window. The non-solvent baths can also act as support, maintain the integrity of the printed structures through buoyance, and are known to increase ink stability.[10] To that end, different hydrophobic alkane solvents were contained in a petri dish and the printing nozzle would traverse underneath the liquid-air interface. One requirement for the solvent was that the printed polymer-metal oxide composite should be immiscible with the bath. The second requirement was that the ethanol of the ink should be miscible with the solvent bath selected. It was expected that removal of ethanol from the printed structure was going to accelerate the ink precipitation kinetics. To verify the feasibility of this printing setup, rheology measurements were carried out where the surfaces of the two plates were covered with ink first and then immersed in the selected non-solvent (Figure 3.3). Plates were kept immersed in the solvent for different amounts of time before being loaded into the rheometer and studied. A similar measurement sequence was performed on the resulting partially precipitated ink.

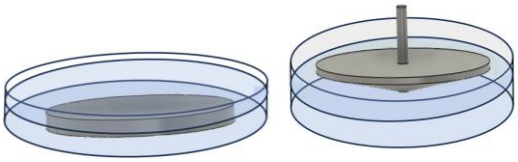

Fig 3.3: Schematic of the setup for rheology measurements of inks immersed in different non-solvent baths. To that end, the two plate surfaces were covered with ink first and then immersed into the non-solvent bath for different amounts of time.

Comparing results displayed in Fig 3.4, hexane as the solvent maximized the achievable moduli as compared to other alkanes. Results suggest that hexane (or other alkane solvents) may diffuse into the printed ink, *e.g.*, swelling the hydrophobic PPO core of the F127 micelles. This diffusion is driven by the concentration gradient and the hexane preferentially mixes with the more hydrophobic PPO block while precipitating the hydrophilic PEO block and the niobia sol, which accounts for the majority volume of the printed components. This would enhance mesophase segregation, increase the modulus of the printed structure and give rise to ink stability. Results are also consistent with ethanol diffusing out of the ink into hexane. Since hexane showed the most promising behavior, it was selected as a solvent bath for DIW of inks.

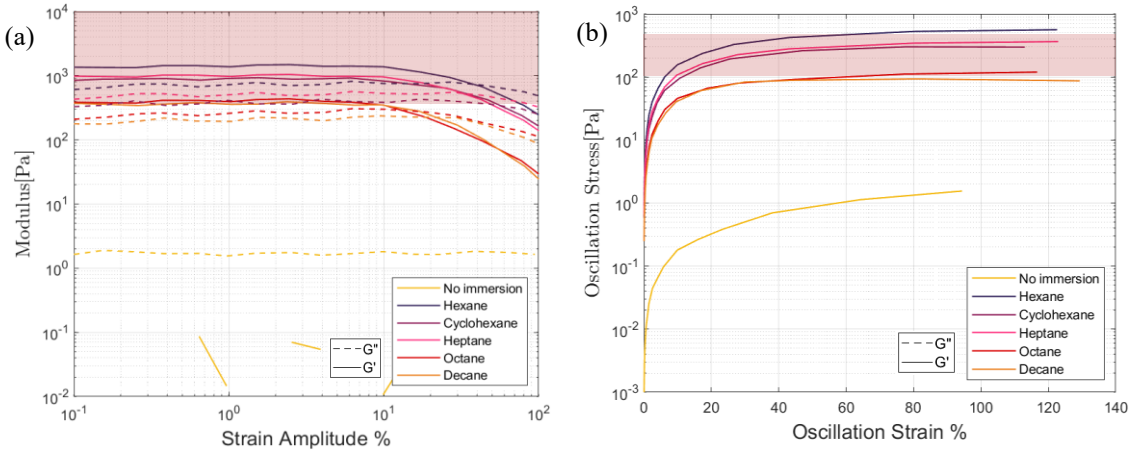

Fig 3.4: At f=1 Hz: (a) Modulus of F127-Niobia inks immersed in different solvents for 5min as a function of amplitude sweep. (b) Oscillation stress in F123-Niobia inks immersed in different non-solvents for 5min as a function of amplitude sweep.

The next step was to decide the printing speed (*i.e*, the speed of the printhead). The printhead speed determines the total amount of time needed to print a complete

woodpile. This decision required knowledge of the precipitation kinetics of the printed ink. Further rheological experiments were not expected to quantitatively define the time taken for each layer to precipitate completely. But combined with the existing literature results were expected to give a qualitative picture of the range to which the printing speed could be set. To investigate the precipitation kinetics, following varying immersion times of plates decorated with ink in hexane further rheological analysis was conducted.

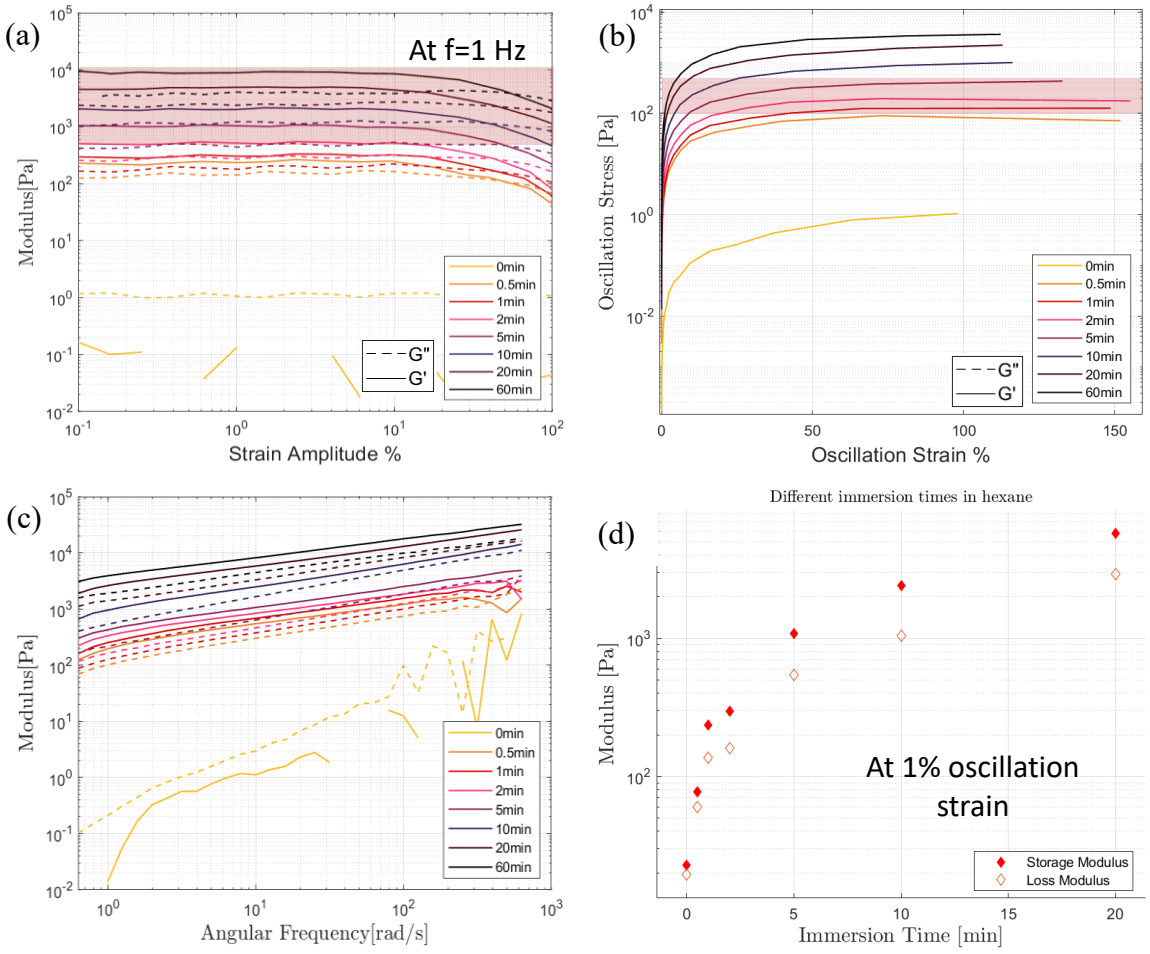

Fig 3.5: At f=1 Hz: (a) Modulus of F127-niobia inks immersed in hexane for different times as measured via amplitude sweeps. (b) Oscillation stress of F123-niobia inks immersed in hexane for different times as measured via amplitude sweeps. At 1% strain: (c) Change in ink moduli as a function of angular frequency. (d) Storage and loss moduli of F127-niobia inks as a function of immersion time in hexane.

To that end, the cone and plate surfaces were covered with ink and immersed in hexane for the following amounts of time: 0 (no immersion), 0.5, 1, 2, 5, 10, 20, and 60 min. After about 20 min of immersion, inks had already completely dried such that it was not generally possible anymore to achieve the truncation gap. This suggested that after about 20 min, the ink had precipitated to a great extent. Fig 3.5 (d) compares storage and loss moduli of inks immersed in hexane for different amounts of time. The modulus monotonically increased with the immersion time, with the greatest increase occurring between no immersion (0 min) and 0.5 min, showing the profound impact that the hexane printing environment exerts on the viscoelastic property of the ink. This data gives an idea of how quickly the ink can reach the printing window. There is not a direct calculation that correlates this time with the printing speed, but it gives an idea of the ink behavior.

It is also important to know the chemistry that drives the ink precipitation. An experiment was performed to study this chemistry. To understand how the solvents interact with the ink and with each other, different compositions of ethanol in hexane as the non-solvent bath were prepared and then used for rheological experiments as described before (Figure 3.6). It was observed from amplitude and flow ramps that increasing the ethanol weight percent in the solvent bath reduced the moduli and viscosity of the immersed ink. An explanation is that the ethanol from the ink diffuses and mixes with the hexane in the solvent bath. When the ethanol weight percent in the solvent bath is increased, there is a decrease in ethanol gradient across the ink and the solvent bath leading to slower diffusion of ethanol from the ink into the solvent bath. Results confirm that ethanol diffusion from ink to the non-solvent bath is a contributor to increasing the ink precipitation rate. As pointed out earlier, there is diffusion of hexane from the bath to the ink regardless of the ethanol concentration in the bath.

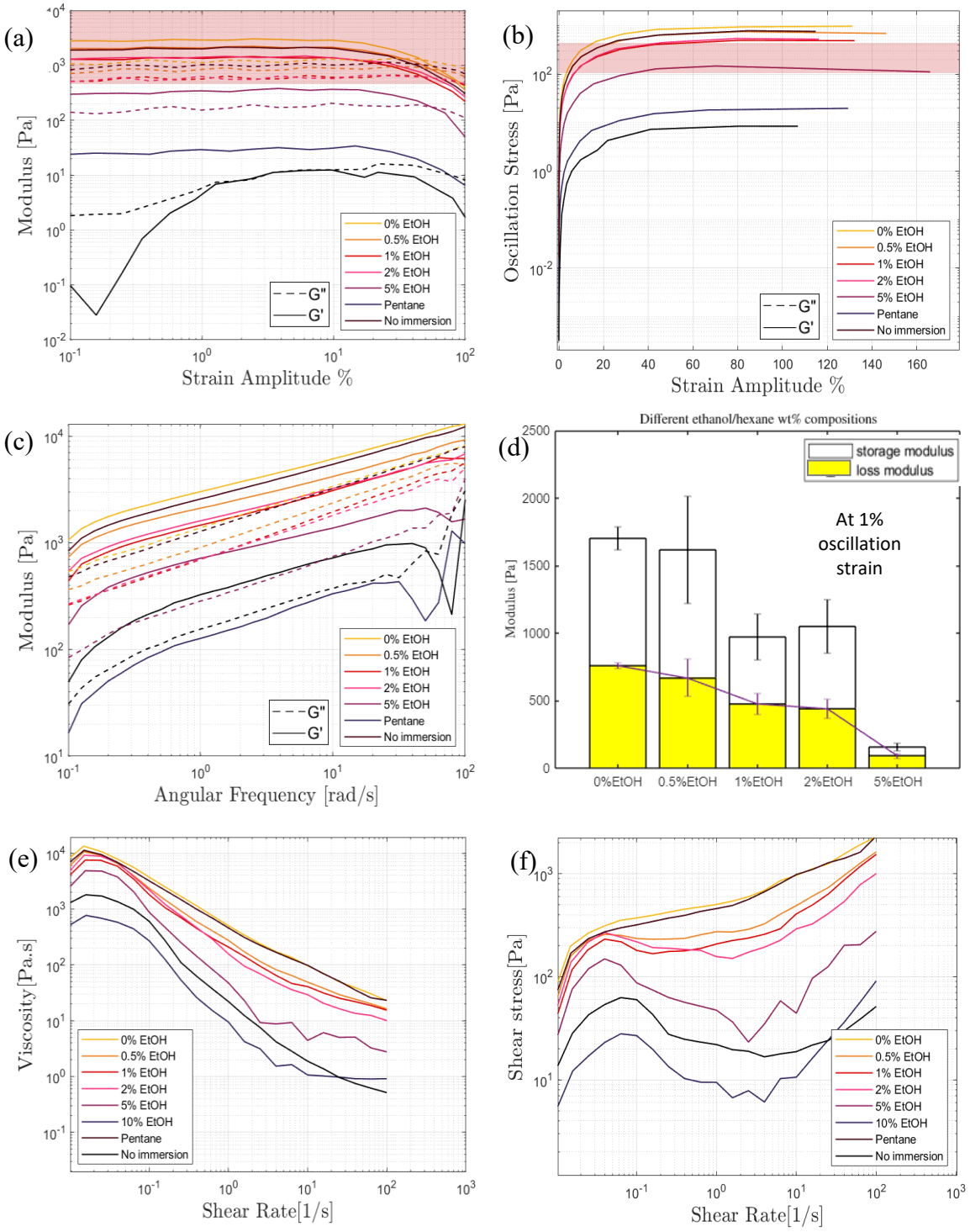

Fig 3.6: Effect of different ramps (amplitude ramps (a,b), frequency ramp (c), flow ramps (e,f)) studied on F127-directed niobia inks immersed in different non-solvent bath compositions – wt% of ethanol in hexane – for 5min. (a) Change in ink moduli as a function of shear amplitude in % (at f=1 Hz). (b) Change in oscillation stress as a function of strain amplitude in % (at f=1 Hz). (c) Change in ink moduli as a function of angular frequency (at 1% strain amplitude). (d) Moduli of inks as a function of different wt% of EtOH/Hexane. (e) Change in ink viscosity as a function of shear rate. (f) Shear stress of inks as a function of shear rate.

From all the rheology experiments described so far it was concluded that both the diffusion of hexane from the bath into the ink and of ethanol from the ink into the bath contribute to the increased modulus of the printed ink.

In Figure 3.7 photos are shown of woodpiles printed at a printing speed of 300mm/min into hexane as a non-solvent bath (a), the resulting polymer-inorganic hybrid after it was taken out of the solvent bath (b), and a woodpile calcined at higher temperature to convert the hybrid material into a niobium oxide.

(a) (b) (c)

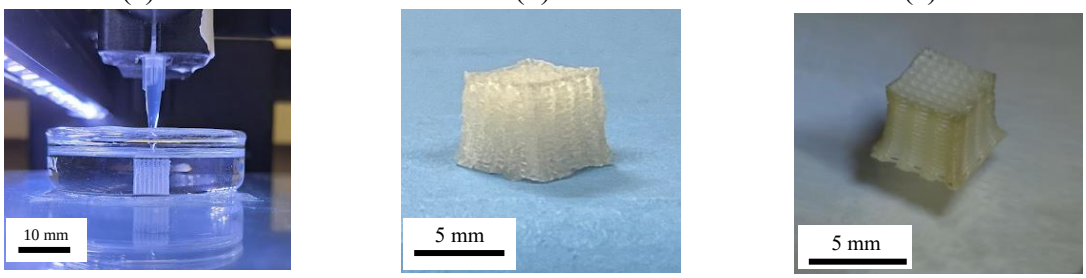

Fig 3.7: Photos of: (a) As-printed Pluronic-niobia hybrid still immersed in the hexane bath; (b) Aged polymer-inorganic hybrid woodpile taken out of the bath; (c) Resulting niobium oxide after calcination at 450 °C.

B. SEM of F127-directed niobia woodpile.

Tube furnace treatment of printed structures at 450 °C decomposes the polymeric Pluronics, leaving behind highly condensed niobia with pores formed by the removal of the PPO block. The SEM image in Figure 3.8a shows a cross-sectional view of struts of a calcined niobium oxide woodpile structure. The struts are printed in an orthogonal manner to each other along the z-axis and each individual strut (circled in Figure 3.8a) consists of four printed layers on top of each other. The SEM image in Figure 3.8b shows hexagonally packed hollow cylinders either standing up or lying down, suggesting successful local mesostructure formation in the struts of DIW printed material with Pluronic F127 BCP self-assembly directing the mesoporous materials

structure. The pore size measured by SEM as the diameter of the hollow cylinders is around 7.1nm.

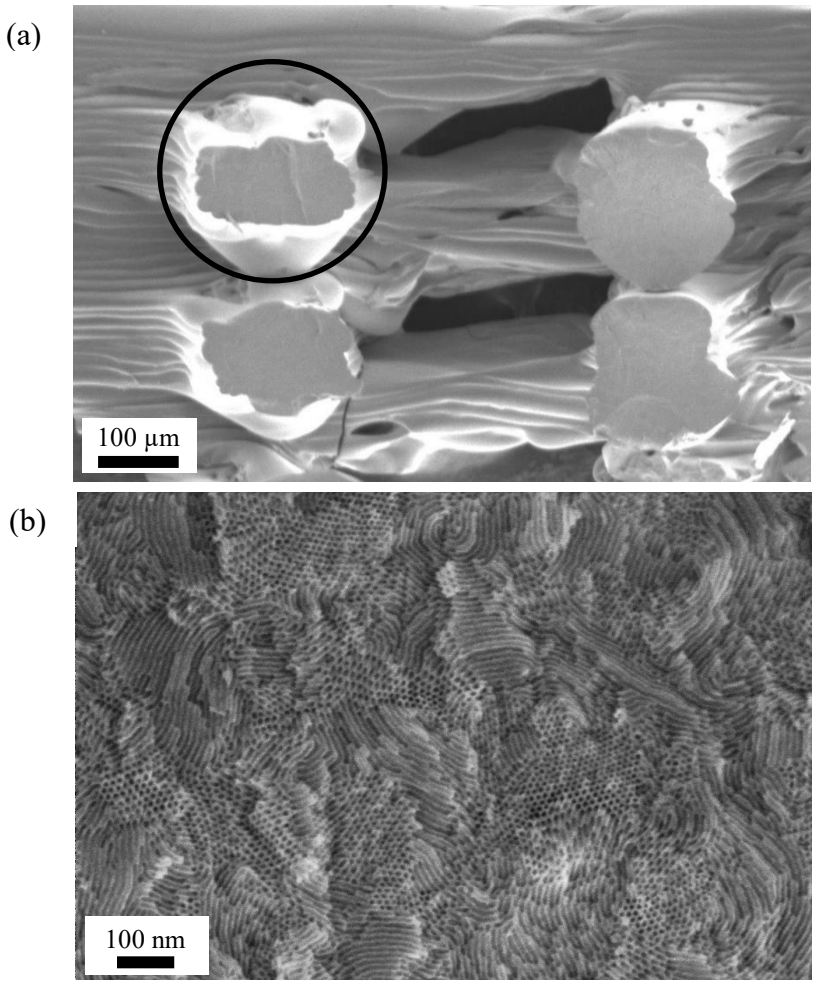

Fig 3.8: (a) Zoomed-in image of cross-sections of 3D printed woodpile struts; (b) SEM image showing hexagonal morphology of F127-directed niobium oxide woodpile structure.

C. Porosity of F127-directed niobia woodpile by N_2 sorption measurements

The porosity measurements were performed using nitrogen sorption desorption. Results of sorption isotherms and resulting pore size distribution are shown in Figure 3.9. The isotherm shows typical type-IV curves with H_1-type hysteresis. The jump in the amount of adsorbed gas at the relative pressure of around 0.67 is consistent with the capillary condensation of adsorbate in the cylindrical mesopores.

The specific surface area of this niobium oxide woodpile came out to be 125.6 m^2/g and with an average pore size narrowly distributed around 8.3 nm using the DFT model.

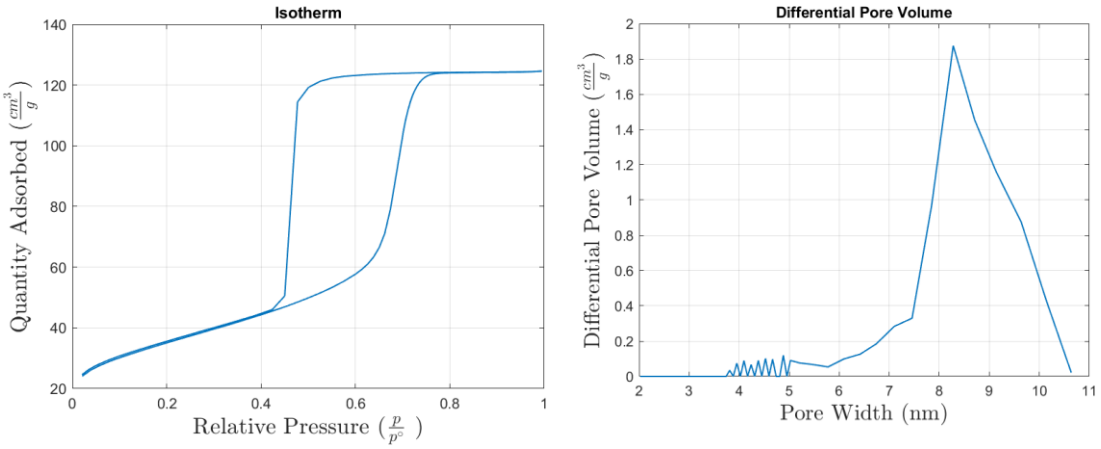

Fig 3.9: Nitrogen sorption/desorption isotherms (left) and resulting pore size distribution (right) for F127-directed niobium oxide woodpile structure from DIW.

D. SAXS of F127-directed niobia

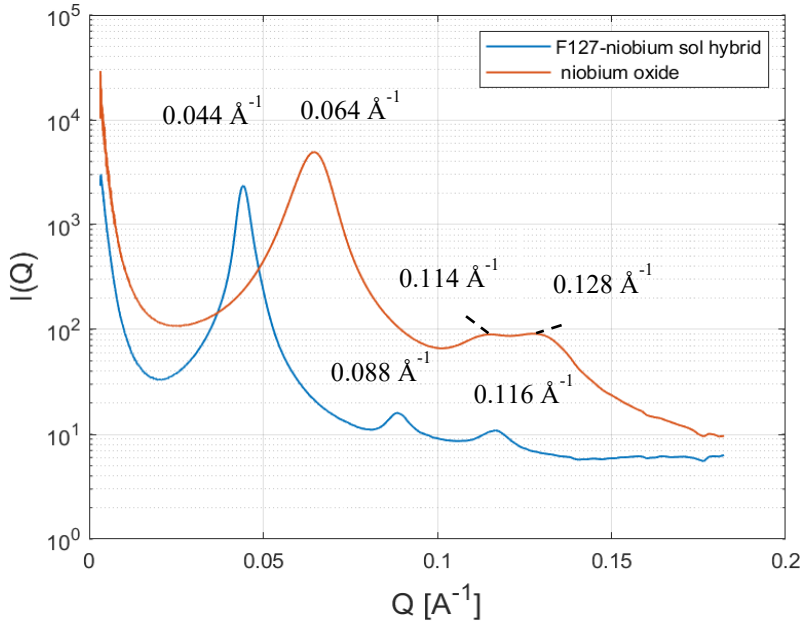

Fig 3.10: SAXS of F127-directed hybrid and resulting niobium oxide confirming a hexagonal morphology from indexing of higher order reflections.

Beyond the local areas probed by SEM, SAXS offers a more global characterization of the underlying mesostructure. Results of SAXS experiments on as-printed F127-directed hybrid material and resulting niobium oxide after calcination at higher temperatures are shown in Figure 3.10. The hybrid was calcined at 450 °C at a ramp rate of 1 °C/min with a dwell time of 3 hrs. Higher order reflections are consistent with a hexagonal lattice for both as-printed and calcined materials, with relative peak positions (q/q^*) appearing at 1, $\sqrt{3}$, and 2. Resulting d-spacing for the two materials as calculated using:

$$d = \frac{2\pi}{Q}$$

provide values of d_{100} of 14.31 nm and 9.75 nm for as-printed and calcined woodpile material, respectively. The observed shrinkage in d spacing as the hybrids is converted to an oxide is expected.

3.2 P123-directed niobia inks and 3 printed structures

Pluronic P123 is a paste-like nonionic surfactant comprised of 20 EO units on both ends and 70 PO units in the middle It is soluble in ethanol at room temperature, leading to micelles, consisting of the hydrophobic PPO block in the core and the hydrophilic PEO end blocks in the corona. Its molar mass is 5800 g/mol, slightly less than half the molar mass of F127.

The hydrophilic PEO blocks form around 30 wt.% of the total chain, the molar mass of

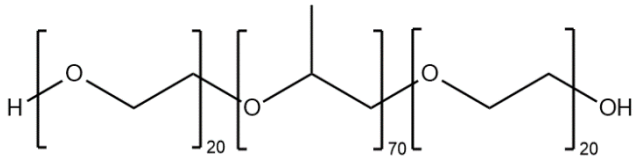

Fig 3.11: Schematic of a Pluronic P123 block copolymer.

which is about 5 times less than the mass of the PEO blocks in F127 polymer. This is expected to result in thinner walls (i.e., a smaller d-spacing) of as-printed materials,

calcined niobium oxides, as well as niobium nitride mesoporous structures after conversion in ammonia (*vide supra*) derived from P123. The motivation behind exploring smaller PEO chain-length Pluronics was to achieve smaller d-spacings that would result in higher confinement of oxide and nitride structures, the latter potentially leading to higher critical magnetic fields (B_c2) of nitride superconductors.

Starting with hybrid films (as in the case of F127 based studies), successful structure formation as evidenced by SEM required higher amounts of niobium precursor as compared to F127-based inks. One possible explanation for this observation is that the smaller wt. % of hydrophilic PEO of P123 (~ 5 times) as compared to F127 may require higher amounts of inorganic precursor to maintain stable mesoporous film walls. Thus adding extra amounts of niobium precursor is necessary. As it turned out, higher amounts of acids were also needed to maintain the self-assembly kinetics.

Since the majority of the P123 chain is hydrophobic, unlike the case of F127, the precipitated ink did not adhere well to the glass petri dish, making it difficult to print a complete woodpile. To overcome this issue, before each printing process, the glass petri dish into which the woodpile was printed needed to be cleaned well in concentrated KOH, followed by silanization with 15 wt.% dichlorodimethylsilane in heptane, to make the glass surface hydrophobic.

This introduced a thin hydrophobic layer of dimethyl siloxane on the petri dish glass surface.[23] We successfully printed woodpile structures using a printhead speed of 300 mm/min (F300 in Gcode), the same as was used for F127-directed niobia inks. The ink was printed at an extrusion rate of 0.1 mm/mm of movement (E 0.1 in Gcode). The P123-niobia woodpile appeared to have a glassy texture as compared to the F127-niobia woodpile.

3.2.1 Results and Discussion

A. Rheology

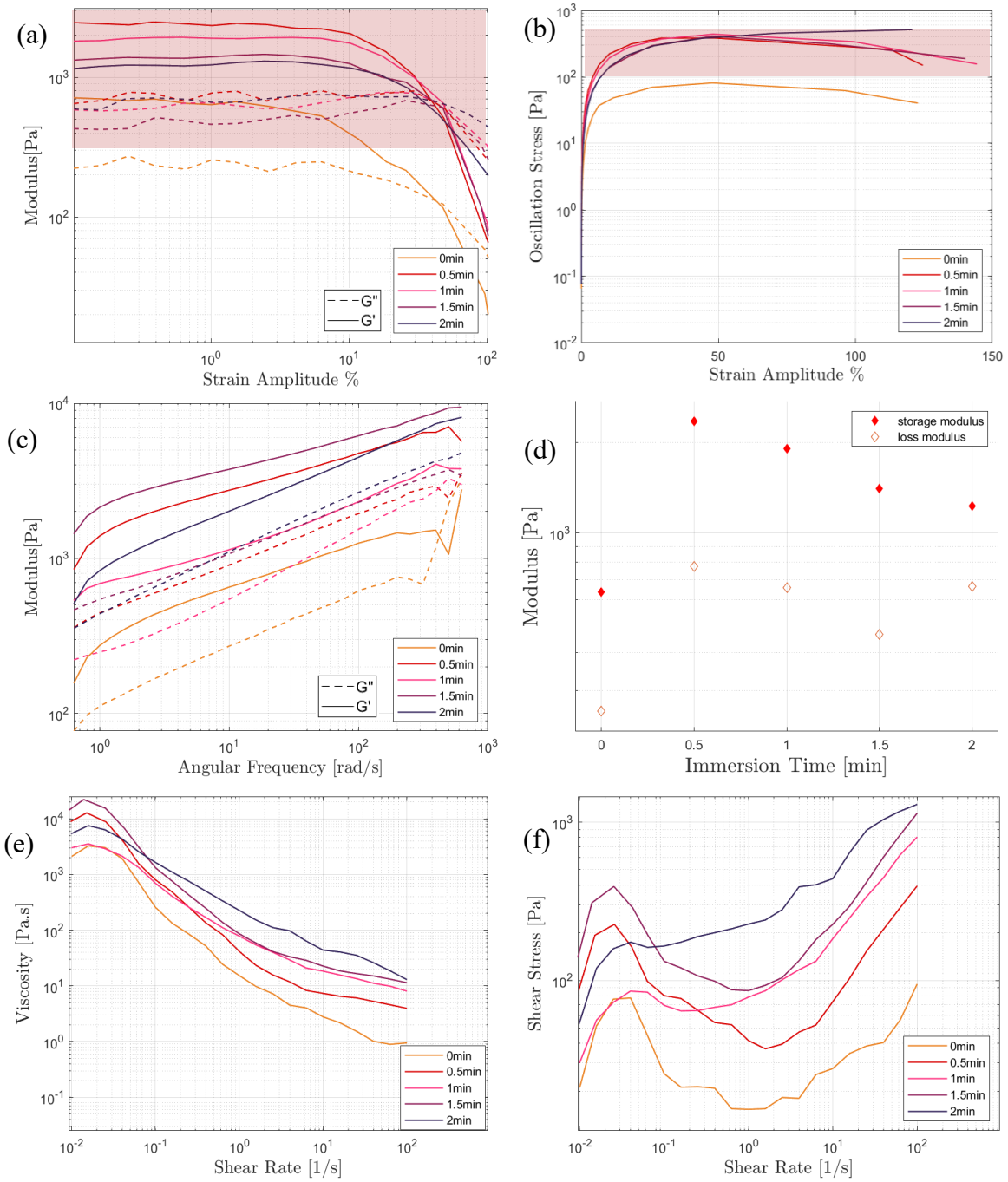

Fig 3.12: Effect of different ramps (amplitude ramps (a,b), frequency ramp (c), flow ramps (e,f)) studied on P123-directed niobia inks immersed in hexane for different amounts of time. (a) Change in ink moduli as a function of strain amplitude % (at f=1 Hz); (b) Change in oscillation stress as a function of strain amplitude in % (at f=1 Hz); (c) Change in ink moduli as a function of angular frequency (at 1% strain amplitude); (d) Moduli of inks as a function of different immersion times; (e) Change in ink viscosity as a function of shear rate; (f) Shear stress of the inks as a function of shear rate.

Results of rheological investigations of P123 directed niobia inks as described for F127 directed inks are summarized in Figure 3.12. Oscillation and frequency sweeps on these inks show that the printing window is reached quickly in the case of P123-directed materials. But the expected trend that the moduli should increase with increasing immersion times was not followed for P123-niobia ink, which can be attributed to fast precipitation so that the hardened ink makes it difficult for the plates to reach the truncation gap before proceeding with the rheology measurements. So, the measurements for higher immersion times (1 min and above) have not been done at the truncation gap of 63 μm.

A flow ramp was also performed on these inks to see the effect of immersion time on the viscosity and shear stress in the samples with increasing shear rates. It was observed that increasing the immersion time is giving rise to increased viscosity and shear stress values which is an indication of increased integrity required to sustain the printed structures.

B. **SEM of P123-directed niobia woodpile**

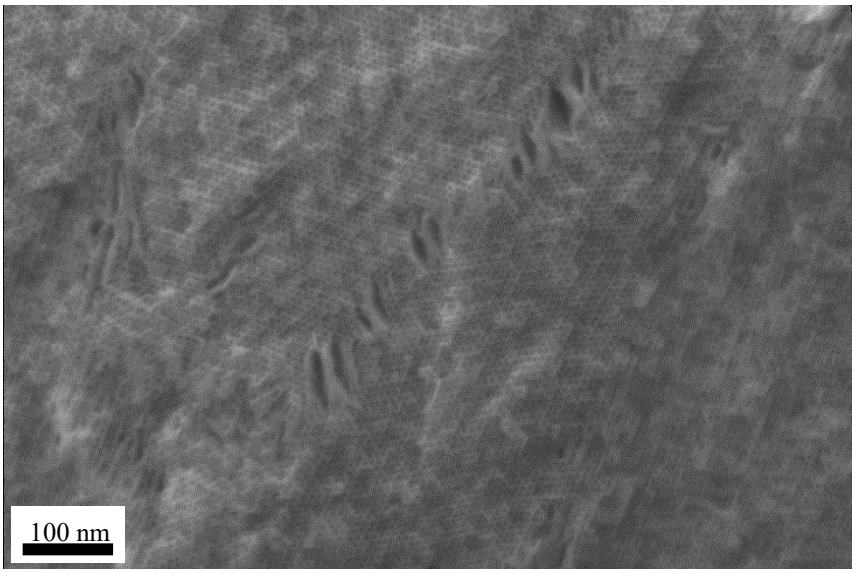

Fig 3.13: SEM image showing hexagonal morphology of P123-directed niobium oxide woodpile structure.

The SEM image in Figure 3.13 of a calcined P123-directed niobium oxide woodpile shows a hexagonal morphology while the pore sizes are very small (~3.7 nm) as compared to the F127 counterparts.

C. Porosity of P123-directed niobia woodpile by N_2 Sorption

The N_2 sorption/desorption measurements showed an isotherm (Figure 3.14) consistent with well-accessible mesopores. The average pore size of this P123-directed niobium oxide woodpile obtained using a DFT model was around 4.7 nm (less than the F127-directed niobia woodpiles which have a pore size of 8.3 nm). The surface area came out to be 127.58 m^2/g.

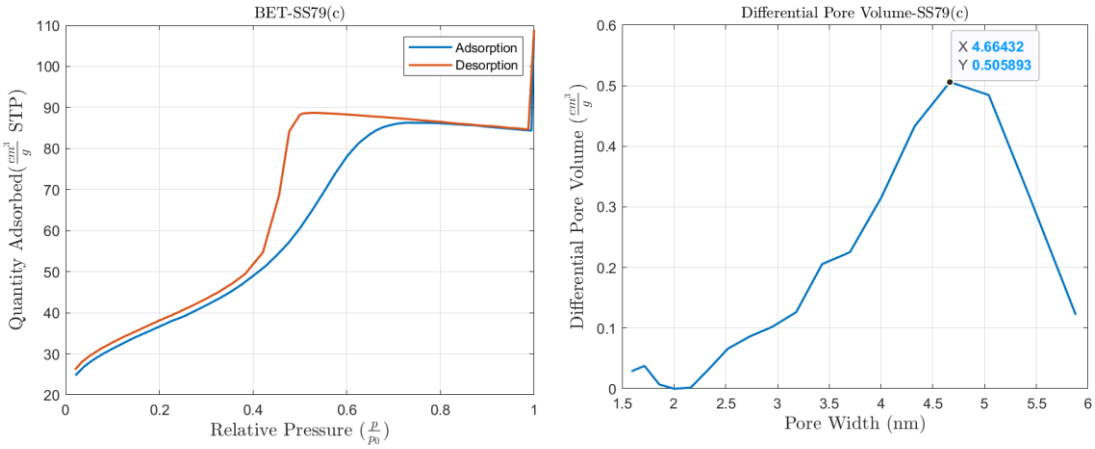

Fig 3.14: Nitrogen sorption/desorption isotherms (left) and resulting pore size distribution (right) of P123-directed niobium oxide woodpile structure from DIW.

D. SAXS measurements on P123-directed Niobia

The SAXS of P123-directed niobium oxide woodpile confirms hexagonal morphology from indexing of higher order reflections. Comparing the SAXS data for the P123-directed niobium oxide woodpile with the F127-directed niobium oxide woodpile clearly demonstrates a decrease in d-spacing (Figure 3.15), suggesting that the wall thickness of the oxide decreased.

- d_{100} spacing of P123-directed niobia woodpile: 7.21 nm.

- d_{100} spacing of P123-directed niobia woodpile: 9.75 nm.

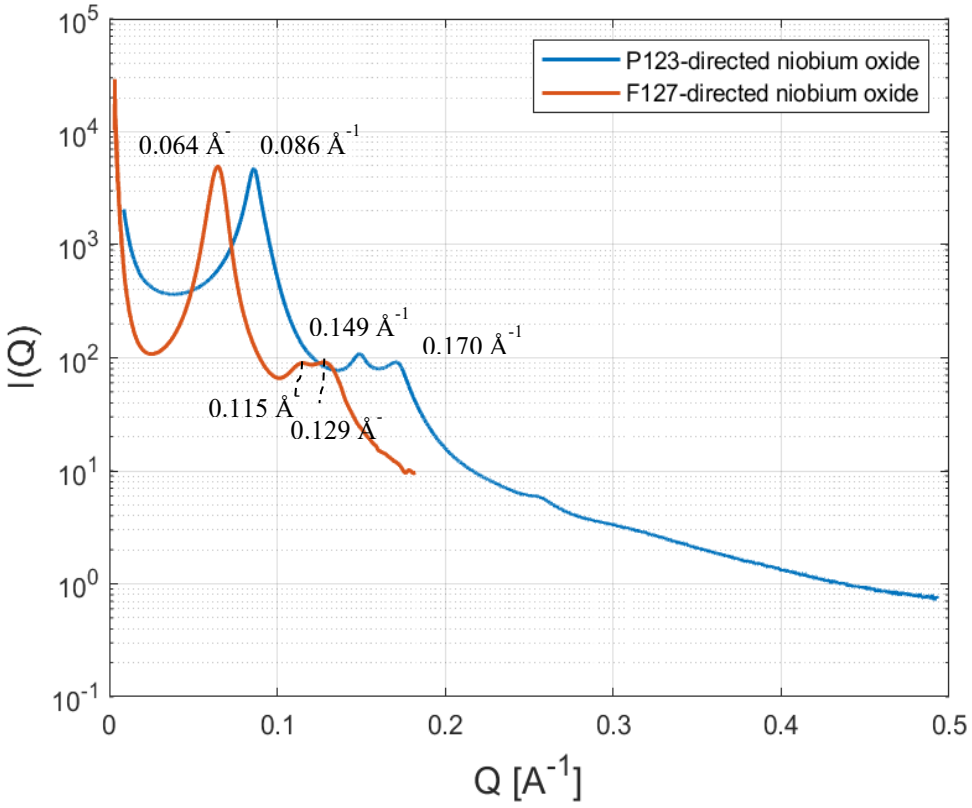

Fig 3.15: Comparison between the d spacing of niobium oxides directed by F127 and P123 using SAXS.

3.3 F127-directed titania inks and 3 printed structures.

Finally, it is demonstrated that DIW of pluronic-sol inks can be extended to other transition metals oxides, notably to titania. To that end, similar to the case of niobium (V) ethoxide equimolar amounts of titanium (IV) isopropoxide were used as the titania precursor to prepare inks. Titanium-based mesoporous structures find use in catalysis, energy storage, sensors, optical materials, and biomedical applications, making them fascinating materials. Titanium nitride is another known (type II) superconductor with applications in high-performance microwave resonators and other low-temperature electronics.

3.3.1 Result and Discussion

A. Rheology

As before, rheology was performed on inks. As compared to F127-directed niobia, the F127-directed titania inks require more immersion time to reach the same value of modulus that is achieved by the former (Figure 3.16). Qualitatively speaking, this reflects longer printing times for F127-directed titania inks. Indeed, each successful titania woodpile took ~3 hrs to print (with a print head speed of 100 mm/min).

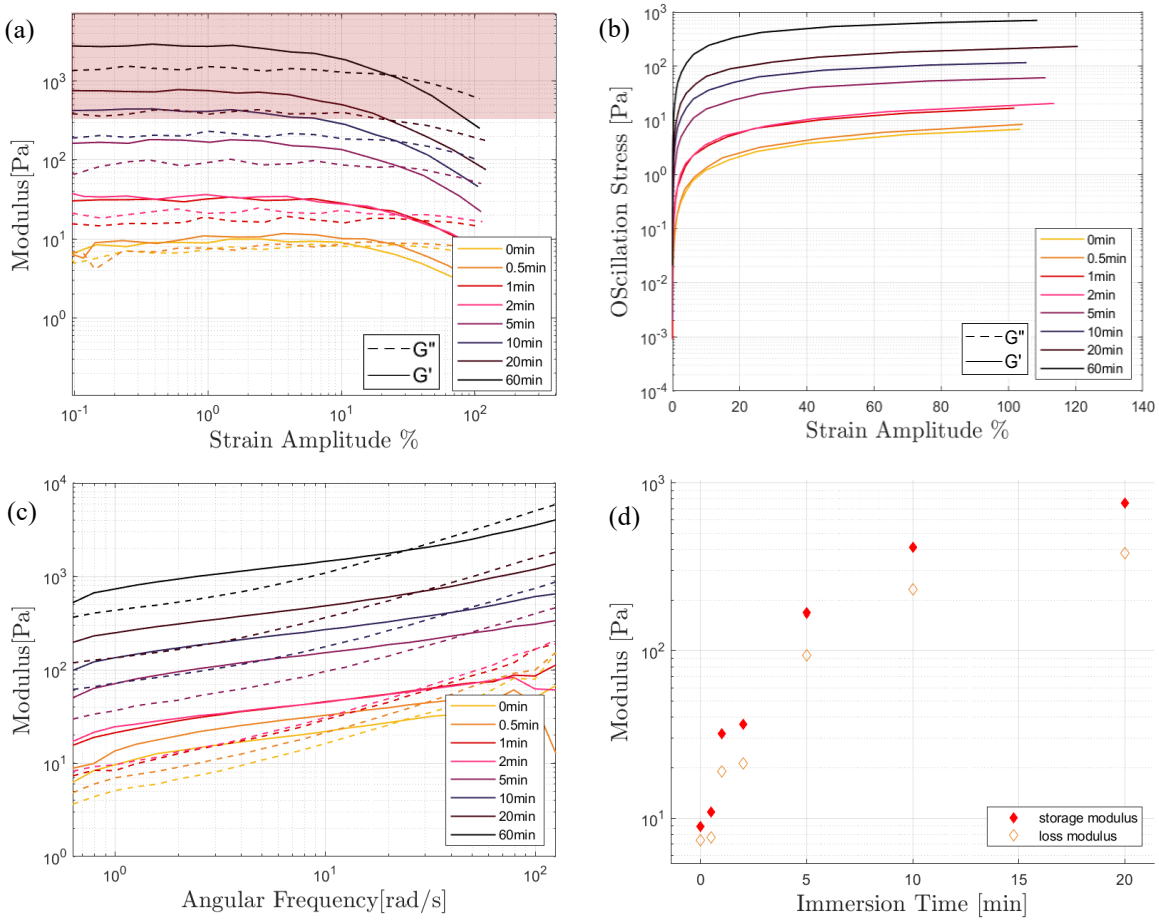

Fig 3.16: Effect of different ramps (amplitude ramps 'a,b' and frequency ramp, 'c') studied on F127-Titania inks immersed in hexane non-solvent baths for different times. (a) Change in ink moduli as a function of strain amplitude in % (at f=1 Hz); (b) Change in oscillation stress as a function of strain amplitude in % (at f=1 Hz); (c) Change in ink moduli as a function of angular frequency (at 1% strain); (d) Moduli of inks as a function of different immersion times.

The rheology data obtained from all three ink systems explored in this thesis was compared in Figure 3.17. The change in modulus as a function of immersion time was compared to see how the three ink systems evolved in modulus with immersion in a hexane bath. This comparison reveals the immersion time required for each ink to reach the printing window. It is observed that P123-Niobia inks reach the printing window within 1 min of immersion time while for higher immersion times, it is not possible to acquire reliable data because the geometry plates don't reach the truncation gap. F127-titania inks take the highest time to reach a modulus in the printing window. It is also reflected in the printing set-up where the printing time is 3hrs per woodpile, compared to F127-Niobia inks which take just 1hr per woodpile.

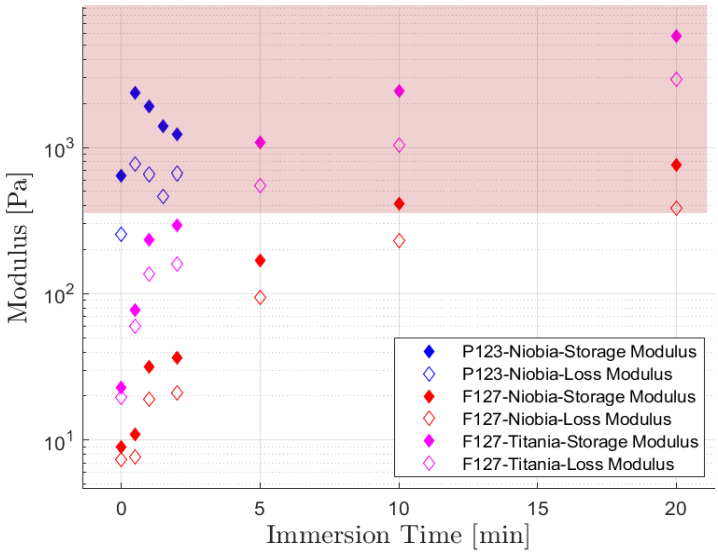

Fig 3.17: Comparison of Modulus of different inks as a function of increasing immersion times in hexane.

B. SEM

The SEM image in Figure 3.18 of a calcined titanium oxide woodpile shows hexagonally packed cylinders either standing up or lying down suggesting successful local mesostructure formation in the DIW printed material with Pluronic F127 BCP self-assembly directing the mesoporous materials structure. The average pore size is 6.2 nm.

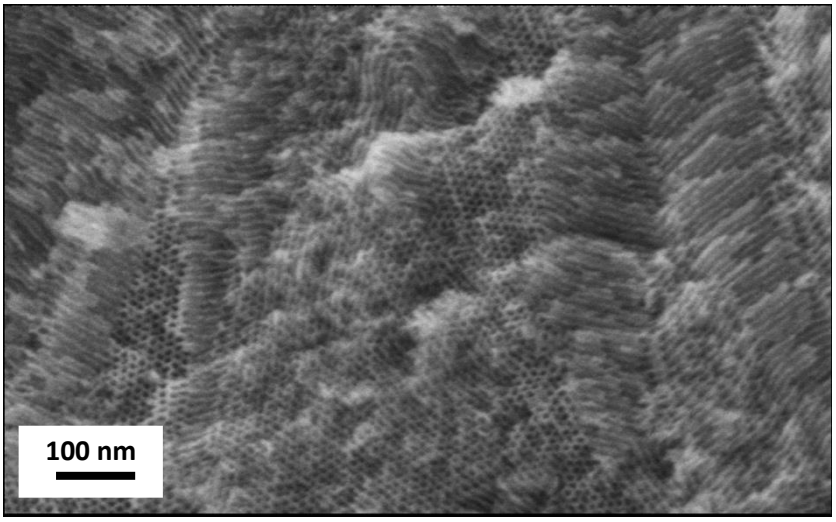

Fig 3.18: SEM image of F127-directed titanium oxide woodpile showing hexagonal morphology.

C. N_2 Sorption – BET

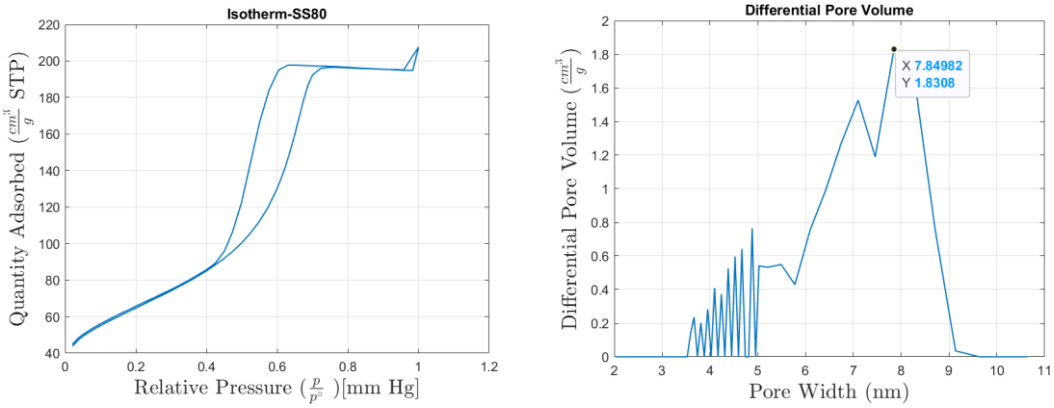

Fig 3.19: Nitrogen sorption/desorption isotherms (left) and resulting pore size distribution (right) for F127-directed titanium oxide woodpile structure from DIW.

The N_2 sorption/desorption measurement results are shown in Figure 3.19, showing isotherms consistent with the existence of accessible mesopores. The average pore size of the F127-directed titania woodpile mesostructure came out to be 7.8 nm (comparable to the F127-directed niobia woodpiles which have a pore size of 8.3 nm).

D. SAXS

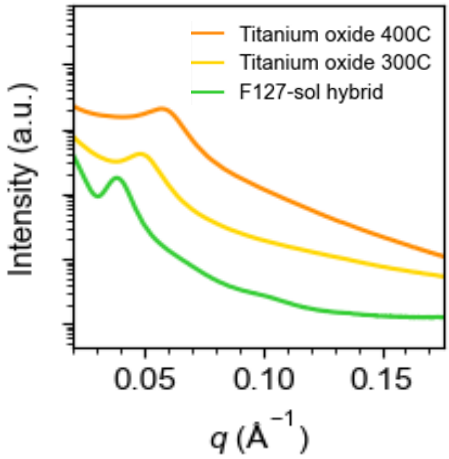

Fig 3.20: SAXS analysis on F127-titania sol hybrid, and titania calcined at different temperatures. Heat treatment and conversion to oxides resulted in shrinkage of d spacing, indicated by q shifting to the right.

SAXS measurements were performed on a hybrid and two oxide samples heated to different temperatures (i.e., 300°C and 400°C) to see the change in structure. It was observed that the q values shifted successively to the right moving from the hybrid to oxides treated to higher temperatures, which is consistent with progressive shrinkage and a resultant decrease in d-spacing going from as-printed hybrids to oxides heat treated to higher and higher temperatures.

E. WAXS

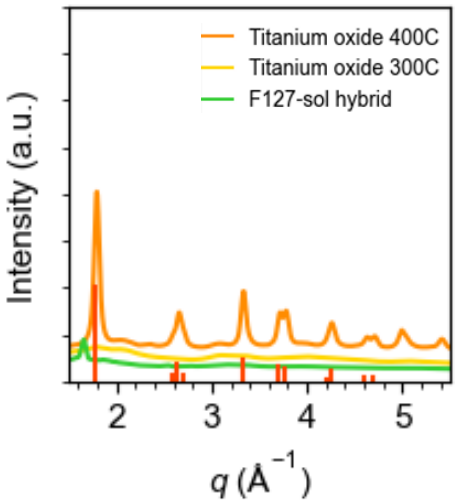

Fig 3.21: XRD data of F127-titania sol hybrid, and titania oxide calcined at different temperatures. Reference show peaks for crystalline titania consistent with anatase.

Titania oxide crystallizes at lower temperatures than niobium oxide. This is confirmed by WAXS measurements (Figure 3.21). Against the amorphous background of the as-printed hybrids and the oxide calcined at 300 °C, the oxide calcined at 400 °C shows crystalline peaks consistent with the anatase phase of TiO_2. The average crystal size of the anatase crystals was calculated to be 8.9 nm using Scherrer analysis. Together with the corresponding SAXS and SEM data, results demonstrate that the printed woodpile calcined at 400 °C is periodically ordered on both the mesoscale and the atomic scale.

3.4 Nitridation of oxides for superconductors

Transition metal compounds exhibit a captivating array of electrical, magnetic, optical, and thermal properties. One such functional example is niobium nitride, a type-II superconductor, which can be prepared from amorphous niobium oxide through two-

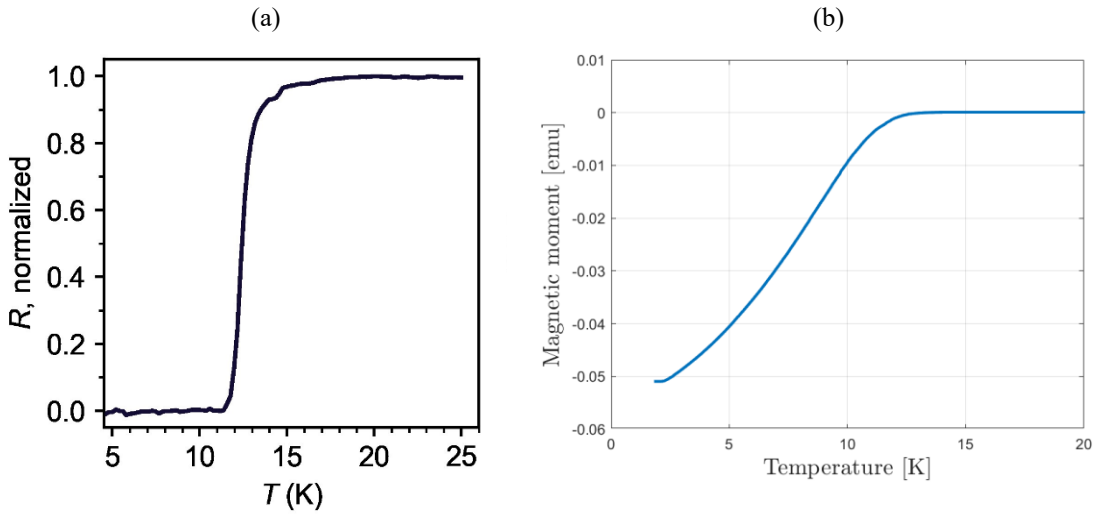

Fig 3.22: (a) Resistance vs Temperature curve (at 0 T) showing superconductivity of NbN, (b) Temperature-dependent magnetization for a superconducting NbN

step thermal processing. Initially, the amorphous niobium oxide undergoes treatment in ammonia at 550 °C, followed by treatment in carburizing gas at 950 °C to achieve the conversion into niobium nitride.

BCP-directed mesoporous transition metal oxides play a vital role in this synthesis, offering well-defined pore structures and high surface areas facilitating the oxide-to-nitride transformation and that serve as a versatile platform for creating mesoporous superconducting nitrides. The controlled nanoscale architecture of these materials allows precise regulation of the nitridation process and facilitates the formation of well-dispersed, interconnected nitride phases. The process involves the calcination of hybrid F127-niobium-sol based hybrid structures in an air environment at 450 °C, yielding porous and amorphous niobium oxide (Nb_2O_5). Subjecting the amorphous niobium oxide to ammonia treatment [24] at 550 °C and subsequently to carburizing gas (mixture of methane, hydrogen, and nitrogen in a ratio of 16:4:80) treatment at 950 °C brings about its transformation into niobium nitride, a metallic material that becomes superconducting at low temperatures.

Low-temperature electrical transport measurements of a resulting 3D printed nitride sample suggested that this indeed happened by revealing a superconducting transition temperature of 12.4 K, as determined from the point where the resistance drops to half the value before the transition. Vibrating sample magnetometry measurements show the printed nitride starts to be diamagnetic around 12.5 K, consistent with the result of the transport measurement. Together the two requirements for a superconductor, that is vanishing resistance and the exclusion of external magnetic fields, are therefore fulfilled. Our 3D printing scheme opens new possibilities for mesostructured superconductors with the freedom of choice of form factor to study emerging phenomena as a result of hierarchical ordering.

Chapter 4: Conclusion and Future Direction

In conclusion, the work described in this thesis successfully combined block copolymer self-assembly with 3D printing techniques to create hierarchically porous structures at both the mesoscale and macroscale. By utilizing commercially available Pluronic-family block copolymers, solution-based direct ink writing was achieved, allowing for the fabrication of tailored structures with tunable pore architectures guided by the self-assembling properties of the block copolymers.

The approach was not limited to a specific transition metal oxide (niobium oxide) but could be expanded to a second oxide (titanium oxide) as well as to a nitride. Specifically, we showcased the conversion of 3D-printed niobium oxide into niobium nitride, which exhibited superconductivity. This achievement not only highlights the potential of the fabrication method to generate quantum materials with customized mesostructures and form factors, but also opens new possibilities in the field of quantum information science.

By enabling the design and synthesis of advanced materials with controlled architectures, form factors, and desired properties, this research paves the way to 3D printed functional materials for various applications, including as catalyst supports and in quantum information technologies. Finally, the work establishes a foundation for the development of innovative advanced materials with tailored mesostructures and form factors, expanding the realm of possibilities for materials design and engineering.

As a future direction, this study can be expanded to synthesize other BCP-directed transition metal oxides opening possibilities of 3D printed structures with intriguing electronic and magnetic properties. Previously studied Pluronic-directed mesoporous metal oxides[18] and multicomponent metal oxides[15] can be further explored to integrate their chemistry to fabricate intricate geometries while preserving the mesoscale properties on a larger, macroscale level. Further investigations can focus on

exploring other 3D printer-compatible block copolymers or other Pluronics with varying compositions and chain lengths that can self-assemble into even more intricate and tailored mesostructures and could enhance the versatility and capabilities of the 3D printing technique. As a direct continuation of this work, further attempts can be taken to tune the superconducting properties by increasing the quantum confinement and optimizing the nitridation process parameters.

The incorporation of functional nanomaterials in the printed mesoporous material would be another interesting platform giving rise to multifunctional nanocomposites with unique properties. The potential of 3D-printed mesostructures and form factors can be explored for applications other than superconductors, including catalyst supports and 3D batteries. More in-depth research is required to enhance the scalability and speed of this printing process. Other additive manufacturing techniques that complement BCP self-assembly can be explored in advancing the fabrication of complicated materials.

References

[1] M. Antonietti and G. A. Ozin, “Promises and Problems of Mesoscale Materials Chemistry or Why Meso?,” *Chemistry – A European Journal*, vol. 10, no. 1, pp. 28–41, 2004, doi: https://doi.org/10.1002/chem.200305009.

[2] J. Livage and C. Sanchez, “Sol-gel chemistry,” *J Non Cryst Solids*, vol. 145, pp. 11–19, 1992, doi: https://doi.org/10.1016/S0022-3093(05)80422-3.

[3] M. Yang, M. J. MacLeod, F. Tessier, and F. J. DiSalvo, “Mesoporous Metal Nitride Materials Prepared from Bulk Oxides,” *Journal of the American Ceramic Society*, vol. 95, no. 10, pp. 3084–3089, 2012, doi: https://doi.org/10.1111/j.1551-2916.2012.05351.x.

[4] S. W. Robbins, H. Sai, F. J. DiSalvo, S. M. Gruner, and U. Wiesner, “Monolithic Gyroidal Mesoporous Mixed Titanium–Niobium Nitrides,” *ACS Nano*, vol. 8, no. 8, pp. 8217–8223, Aug. 2014, doi: 10.1021/nn502548m.

[5] G. J. de A. A. Soler-Illia, E. L. Crepaldi, D. Grosso, and C. Sanchez, “Block copolymer-templated mesoporous oxides,” *Curr Opin Colloid Interface Sci*, vol. 8, no. 1, pp. 109–126, 2003, doi: https://doi.org/10.1016/S1359-0294(03)00002-5.

[6] E. Shukrun Farrell, Y. Schilt, M. Y. Moshkovitz, Y. Levi-Kalisman, U. Raviv, and S. Magdassi, “3D Printing of Ordered Mesoporous Silica Complex Structures,” *Nano Lett*, vol. 20, no. 9, pp. 6598–6605, Sep. 2020, doi: 10.1021/acs.nanolett.0c02364.

[7] C. Sanchez, C. Boissière, D. Grosso, C. Laberty, and L. Nicole, “Design, Synthesis, and Properties of Inorganic and Hybrid Thin Films Having

Periodically Organized Nanoporosity," *Chemistry of Materials*, vol. 20, no. 3, pp. 682–737, Feb. 2008, doi: 10.1021/cm702100t.

[8] Y. Zhang *et al.*, "Mesoporous bioactive glass nanolayer-functionalized 3D-printed scaffolds for accelerating osteogenesis and angiogenesis," *Nanoscale*, vol. 7, no. 45, pp. 19207–19221, 2015, doi: 10.1039/C5NR05421D.

[9] G. M. Gratson, M. Xu, and J. A. Lewis, "Direct writing of three-dimensional webs," *Nature*, vol. 428, no. 6981, p. 386, 2004, doi: 10.1038/428386a.

[10] J. A. Lewis, "Direct ink writing of 3D functional materials," *Adv Funct Mater*, vol. 16, no. 17, pp. 2193–2204, Nov. 2006, doi: 10.1002/adfm.200600434.

[11] M. A. S. R. Saadi *et al.*, "Direct Ink Writing: A 3D Printing Technology for Diverse Materials," *Advanced Materials*, vol. 34, no. 28, p. 2108855, 2022, doi: https://doi.org/10.1002/adma.202108855.

[12] J. A. Lewis, J. E. Smay, J. Stuecker, and J. Cesarano, "Direct Ink Writing of Three-Dimensional Ceramic Structures," *Journal of the American Ceramic Society*, vol. 89, no. 12, pp. 3599–3609, 2006, doi: https://doi.org/10.1111/j.1551-2916.2006.01382.x.

[13] J. G. Álvarez-Ramírez *et al.*, "Phase behavior of the Pluronic P103/water system in the dilute and semi-dilute regimes," *J Colloid Interface Sci*, vol. 333, no. 2, pp. 655–662, 2009, doi: https://doi.org/10.1016/j.jcis.2009.01.068.

[14] P. Alexandridis, J. F. Holzwarth, and T. A. Hatton, "Micellization of Poly(ethylene oxide)-Poly(propylene oxide)-Poly(ethylene oxide) Triblock Copolymers in Aqueous Solutions: Thermodynamics of Copolymer Association," *Macromolecules*, vol. 27, no. 9, pp. 2414–2425, Apr. 1994, doi: 10.1021/ma00087a009.

[15] J. Fan, S. W. Boettcher, and G. D. Stucky, "Nanoparticle assembly of ordered multicomponent mesostructured metal oxides via a versatile sol-gel process,"

Chemistry of Materials, vol. 18, no. 26, pp. 6391–6396, Dec. 2006, doi: 10.1021/cm062359d.

[16] L. Li *et al.*, "Hierarchical Co-Assembly Enhanced Direct Ink Writing," *Angewandte Chemie*, vol. 130, no. 18, pp. 5199–5203, Apr. 2018, doi: 10.1002/ange.201800593.

[17] D. Zhao, Q. Huo, J. Feng, B. F. Chmelka, and G. D. Stucky, "Nonionic Triblock and Star Diblock Copolymer and Oligomeric Surfactant Syntheses of Highly Ordered, Hydrothermally Stable, Mesoporous Silica Structures," *J Am Chem Soc*, vol. 120, no. 24, pp. 6024–6036, Jun. 1998, doi: 10.1021/ja974025i.

[18] P. Yang, D. Zhao, D. I. Margolese, B. F. Chmelka, and G. D. Stucky, "Generalized syntheses of large-pore mesoporous metal oxides with semicrystalline frameworks," *Nature*, vol. 396, no. 6707, pp. 152–155, 1998, doi: 10.1038/24132.

[19] L. Li *et al.*, "Supporting Information Hierarchical Co-Assembly Enhanced Direct Ink Writing."

[20] P. A. Beaucage, E. M. Susca, S. M. Gruner, and U. B. Wiesner, "Discovering Synthesis Routes to Hexagonally Ordered Mesoporous Niobium Nitrides Using Poloxamer/Pluronics Block Copolymers," *Chemistry of Materials*, vol. 29, no. 21, pp. 8973–8977, Nov. 2017, doi: 10.1021/acs.chemmater.7b03834.

[21] Ramli, Hairunnisa, Zainal, Nurul Fatahah Asyqin, Hess, Michael and Chan, Chin Han. "Basic principle and good practices of rheology for polymers for teachers and beginners" *Chemistry Teacher International*, vol. 4, no. 4, 2022, pp. 307-326. https://doi.org/10.1515/cti-2022-0010.

[22] Y. Liu, H. H. Winter, and S. L. Perry, "Linear viscoelasticity of complex coacervates," *Adv Colloid Interface Sci*, vol. 239, pp. 46–60, 2017, doi: https://doi.org/10.1016/j.cis.2016.08.010.

[23] B. Seed, “Silanizing Glassware,” *Curr Protoc Mol Biol*, vol. 28, no. 1, p. A.3B.1-A.3B.2, 1994, doi: https://doi.org/10.1002/0471142727.mba03bs28.

[24] P. A. Beaucage, R. B. van Dover, F. J. DiSalvo, S. M. Gruner, and U. Wiesner, “Superconducting Quantum Metamaterials from Convergence of Soft and Hard Condensed Matter Science,” *Advanced Materials*, vol. 33, no. 26, Jul. 2021, doi: 10.1002/adma.202006975.

[25] J. Huang, Q. Qin, and J. Wang, “A Review of Stereolithography: Processes and Systems,” *Processes*, vol. 8, no. 9, 2020, doi: 10.3390/pr8091138.

[26] MakerVerse. https://www.makerverse.ai/technologies-fdm (Accessed on 07/15/2023).

[27] L. del-Mazo-Barbara and M.-P. Ginebra, “Rheological characterisation of ceramic inks for 3D direct ink writing: A review,” *J Eur Ceram Soc*, vol. 41, no. 16, pp. 18–33, 2021, doi: https://doi.org/10.1016/j.jeurceramsoc.2021.08.031.

[28] P. Pandey, A. Nayak, and M. Taufik, “Evaluation of mathematical models for surface roughness prediction of PolyJet 3D printed parts,” *Advances in Materials and Processing Technologies*, vol. 0, no. 0, pp. 1–10, 2022, doi: 10.1080/2374068X.2022.2097416.

[29] M. C. Orilall and U. Wiesner, “Block copolymer based composition and morphology control in nanostructured hybrid materials for energy conversion and storage: solar cells, batteries, and fuel cells,” *Chem. Soc. Rev.*, vol. 40, no. 2, pp. 520–535, 2011, doi: 10.1039/C0CS00034E.

[30] A. Naharros-Molinero, M. Á. Caballo-González, F. J. de la Mata, and S. García-Gallego, “Direct and Reverse Pluronic Micelles: Design and Characterization of Promising Drug Delivery Nanosystems,” *Pharmaceutics*, vol. 14, no. 12, 2022, doi: 10.3390/pharmaceutics14122628.